Potent but transient immunosuppression of T-cells is a general feature of CD71$^+$ erythroid cells

Tomasz M. Grzywa[1,2,3], Anna Sosnowska[1,4], Zuzanna Rydzynska[1], Michal Lazniewski[5,6], Dariusz Plewczynski[5,7], Klaudia Klicka[2,8], Milena Malecka-Gieldowska[9], Anna Rodziewicz-Lurzynska[10], Olga Ciepiela[9], Magdalena Justyniarska[1], Paulina Pomper[11], Marcin M. Grzybowski[11], Roman Blaszczyk[11], Michal Wegrzynowicz[12], Agnieszka Tomaszewska[13], Grzegorz Basak[13], Jakub Golab[1,14*], Dominika Nowis[1,3*]

[1]Department of Immunology, Medical University of Warsaw, Warsaw, Poland
[2]Doctoral School of the Medical University of Warsaw, Warsaw, Poland
[3]Laboratory of Experimental Medicine, Medical University of Warsaw, Warsaw, Poland
[4]Postgraduate School of Molecular Medicine, Medical University of Warsaw, Warsaw, Poland
[5]Laboratory of Functional and Structural Genomics, Centre of New Technologies, University of Warsaw, Warsaw, Poland
[6]Centre for Advanced Materials and Technologies, Warsaw University of Technology, Warsaw, Poland
[7]Faculty of Mathematics and Information Science, Warsaw University of Technology, Warsaw, Poland
[8]Department of Methodology, Medical University of Warsaw, Warsaw, Poland
[9]Department of Laboratory Medicine, Medical University of Warsaw, Warsaw, Poland
[10]Central Laboratory, University Clinical Center of Medical University of Warsaw, Warsaw, Poland
[11]OncoArendi Therapeutics, Warsaw, Poland
[12]Laboratory of Molecular Basis of Neurodegeneration, Mossakowski Medical Research Institute, Polish Academy of Sciences, Warsaw, Poland
[13]Department of Hematology, Transplantation and Internal Medicine, Medical University of Warsaw, Warsaw, Poland
[14]Centre of Preclinical Research, Medical University of Warsaw, Warsaw, Poland

Keywords: CD71$^+$ erythroid cells, erythroid progenitor cells, anemia, arginase, reactive oxygen species, immunosuppression, erythropoiesis, phenylhydrazine

Running title: CECs and immunosuppression

*corresponding authors:
Jakub Golab, M.D., Ph.D.
e-mail: jakub.golab@wum.edu.pl

Dominika Nowis, M.D., Ph.D.
e-mail: dominika.nowis@wum.edu.pl

Department of Immunology
Medical University of Warsaw
5 Nielubowicza Str.
02-097 Warsaw, Poland
Phone: +48-5992199

Abstract

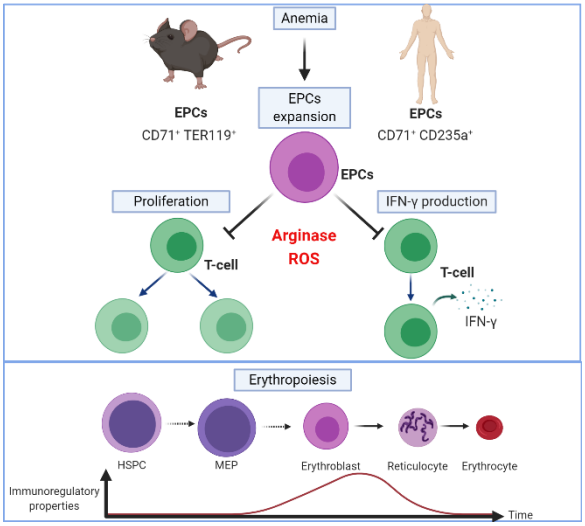

$CD71^{+}$ erythroid cells (CECs) have been recently recognized in both neonates and cancer patients as potent immunoregulatory cells. Here, we show that in mice early-stage CECs expand in anemia, have high levels of arginase 2 (ARG2) and reactive oxygen species (ROS). In the spleens of anemic mice, CECs expansion-induced L-arginine depletion suppresses T-cell responses. In humans with anemia, CECs expand and express ARG1 and ARG2 that suppress T-cells IFN-γ production. Moreover, bone marrow CECs from healthy human donors suppress T-cells proliferation. CECs differentiated from peripheral blood mononuclear cells potently suppress T-cell activation, proliferation, and IFN-γ production in an ARG- and ROS-dependent manner. These effects are the most prominent for early-stage CECs ($CD71^{high}CD235a^{dim}$ cells). The suppressive properties disappear during erythroid differentiation as more differentiated CECs and mature erythrocytes lack significant immunoregulatory properties. Our studies provide a novel insight into the role of CECs in the immune response regulation.

Introduction

CD71$^+$ erythroid cells (CECs) normally reside in the bone marrow and are progenitors and precursors to over 2×10^{11} of oxygen-transporting red blood cells (RBCs) generated per day[1]. In mice, when steady-state erythropoiesis becomes insufficient to meet increased tissue oxygen demands, CECs are released from the bone marrow to the circulation and expand in the extramedullary hematopoietic sites. In humans, increased RBCs damage or loss of blood is compensated by increased erythropoietic activity in the bone marrow. Recent studies revealed an unexpected complexity of CECs functions. CECs arose as a relevant population of cells regulating immunity[2-5]. Initially, CECs were reported to suppress both innate and humoral immune responses in neonates[4,6,7] and it was suggested that their immunomodulatory functions are restricted to early life events[4]. However, further studies revealed a crucial role of CECs in the regulation of multiple phenomena such as fetomaternal tolerance[8], immune response in cancer patients[9,10], systemic inflammation in colitis[11], and anti-viral response in human immunodeficiency virus (HIV) infection[12], as well as SARS-CoV-2-induced disease (COVID-19)[13]. It has been reported that CD45$^+$ CECs induced by advanced tumors inhibit CD8$^+$ and CD4$^+$ T-cell proliferation and impair antimicrobial immunity[10]. Interestingly, the authors demonstrated that CECs from mice with acute hemolytic anemia, induced by systemic phenylhydrazine (PHZ) administration, are not immunosuppressive as compared with CECs from tumor-bearing mice[10]. This could lead to the conclusion that only CECs in newborns and patients with advanced cancer have robust immunosuppressive properties. In this study, we provide evidence that CECs in anemic mice do have immunoregulatory properties, but PHZ used to induce hemolysis affects the mechanisms of immune suppression used by these cells masking their phenotype. Moreover, we

comprehensively elucidate the role of CECs in the regulation of immune response in both mice and humans and demonstrate that immunomodulatory properties of CECs are robust but transient and disappear during their maturation.

Results

Early-stage CECs expand in the spleens of anemic mice

We initially compared the expansion of CECs in 3 days old neonatal and adult anemic mice (Fig. 1a). Non-hemolytic anemia (NHA) was induced by phlebotomy and hemolytic anemia (HA) was induced either by administration of PHZ (HA-PHZ) or anti-TER119 antibodies (HA-TER119) (see Supplementary Fig. 1 for hematological parameters of these mice). Since in mice stress erythropoiesis rely on the erythropoietic activity of the spleen[14,15], we assessed CECs expansion in this organ. CECs expanded in the spleens of anemic mice as compared with controls but were significantly less frequent than in neonatal mice (Fig. 1b). However, CECs numbers in the spleen were substantially higher in anemic mice than in neonates or controls (Fig. 1c). The percentage of CECs increased also in the blood of anemic mice (Supplementary Fig. 2a) but remained unchanged in the bone marrow (Supplementary Fig. 2b). Recent studies indicated that CECs at the earliest stages of differentiation express CD45 and more potently suppress immune response[9,10]. The proportion of $CD45^+$ to $CD45^-$ CECs was the highest in HA-PHZ mice and the lowest in neonatal mice (Fig. 1d). Analysis of developmental stages of CECs based on cell size and CD44 levels (Fig. 1e)[16] revealed enrichment of less differentiated CECs in anemic mice compared to non-anemic controls (Fig. 1f, Supplementary Fig. 2c). These early-stage CECs expressed CD45 (Fig. 1g,h) and were predominantly erythroid progenitors before enucleation (Fig. 1i).

The T-cell immune response is impaired in anemic mice

Next, we sought to determine whether the expansion of early-stage CECs induced by anemia might impair the function of the immune system. To this end, we assessed selected functionalities of myeloid cells, B-cells, and T-cells in control and anemic mice. In contrast to neonatal mice[4,6], production of TNF-α by splenic $CD11b^+$ cells after stimulation with heat-killed *E. coli* (HKEc) (Supplementary Fig. 3a,b) or the concentration of anti-ovalbumin (OVA) IgG antibodies after OVA-ALUM immunization (Supplementary Fig. 3c,d) was unimpaired in adult anemic mice as compared with healthy controls. Intriguingly, we found that the proliferation of adoptively transferred SIINFEKL-specific OT-I T-cells in response to OVA stimulation was decreased in the spleen of NHA mice compared to healthy controls (Fig. 2a,b).

Since the expansion of $CD71^+$ cells was the most substantial in the spleens of anemic mice (Supplementary Fig. 3e) and the ratio of CECs number to T-cells number was significantly increased in anemia (Supplementary Fig. 3f,g), we hypothesized that CECs might be responsible for T-cells suppression. Indeed, CECs isolated from the spleens of both HA and NHA anemic mice (Fig. 2c, Supplementary Fig. 4a) suppressed the proliferation of $CD4^+$ T-cells that were activated with anti-CD3/CD28 beads (Fig. 2d). Altogether, these data document a rather selective impairment of T-cell response by CECs in anemic mice.

Murine CECs have high ROS levels and express ARG2

Both ROS generation and expression of L-Arg-degrading enzymes were previously identified as the effectors of the immunoregulatory activity of neonatal CECs[4,17].

Accordingly, we found that both cytoplasmic and nuclear ROS levels were higher in anemia-induced CECs as compared with mature RBCs (Fig. 3a, Supplementary Fig. 5a,b). ROS reached the highest values in the CECs at the earliest stages of their maturation (Supplementary Fig. 5c,d) i.e. in $CD45^+$ CECs (Supplementary Fig. 5e,f). Interestingly, in contrast to human CECs[13], ROS levels in murine CECs, including $CD45^+$ CECs, were significantly lower than in the cells of non-erythroid lineages such as myeloid cells or T-cells (Fig. 3b).

Murine CECs expressed ARG2, a mitochondrial arginase isoform (Fig. 3c,d), but had almost undetectable cytosolic ARG1 based on intracellular staining (Fig. 3e) as well as enhanced Yellow Fluorescent Protein (eYFP) signal in reporter B6.129S4-$Arg1^{tm1Lky}$/J mice that express eYFP under *Arg1* promoter (Fig. 3f,g). Similar to ROS, the levels of ARG1 and ARG2 were the highest in early-stage CECs and consequently decreased during maturation (Supplementary Fig. 6a-g). Intriguingly, while the level of ARG2 (Fig. 3c), as well as the percentage of $ARG2^+$ CECs, were similar in all groups (Fig. 3d), the fraction of $ARG1^+$ cells was substantially higher in HA-PHZ mice as determined by intracellular staining (Fig. 3e). This finding seems counterintuitive considering that ARG-dependent degradation of L-arginine leads to T-cell suppression[18,19], and we did not observe the suppression of T-cells in HA-PHZ mice *in vivo* (Fig. 2b). Moreover, CECs from HA-PHZ mice exerted the weakest suppressive effects on T-cells proliferation (Fig. 2d). Increased expression of ARG1 in HA-PHZ CECs was further confirmed by ARG1 mRNA detection (Supplementary Fig. 7a) and in reporter B6.129S4-$Arg1^{tm1Lky}$/J mice (Fig. 3g,h) indicating that flow cytometry findings were not artifactual. HA-PHZ CECs had increased expression of ARG2 mRNA as compared with NHA CECs (Supplementary Fig. 7b), but no increase in ARG2 protein levels was observed (Fig. 3d). Surprisingly, despite robust

upregulation of ARG1 levels, total arginase activity in both CECs isolated from HA-PHZ mice and CECs-conditioned medium was lower even than that in CECs from NHA mice (Fig. 3i,j). Moreover, CECs cultured *ex vivo* in the presence of PHZ strongly upregulated ARG1 expression (Fig. 3k,l). Then, we sought to confirm whether PHZ is responsible for the attenuation of CECs immunoregulatory properties. Indeed, we found that CECs isolated from NHA lose their suppressive effects on T-cells proliferation in the presence of PHZ (Supplementary Fig. 8a,b).

PHZ targets arginase and suppresses its activity

Increased expression with a concomitant decrease in arginase activity suggested an interaction between PHZ and arginase. Further studies showed that indeed PHZ inhibits the activity of recombinant human ARG1 and ARG2, with an IC_{50} of 1017 μM and 61 μM, respectively (Fig. 4a). However, PHZ did not affect the production of nitric oxide (NO) by nitric oxide synthase, which is also using L-arginine as a substrate (Fig. 4b). To elucidate how PHZ interacts with ARG1 and ARG2 a molecular docking simulation was carried out with PHZ, L-arginine as well as 2-amino-6-borono-2-(2-(piperidin-1-yl)ethyl)hexanoic acid (ABH) that is a strong ARG1 inhibitor[20]. PHZ binds to the active sites of all arginases, where it forms several polar interactions involving D128, D232, or T246 (Supplementary Fig. 9a). Thus, it may block the entry of other molecules to the active site. However, predicted binding energies suggest that among the tested ligands PHZ has the weakest affinity for arginases, and thus a significant concentration of this compound may be required to induce any biological effect, which indeed is the case *in vivo*. The transient nature of interactions between PHZ and arginases was also confirmed by a short 100 ns MD simulation (Supplementary Fig. 9b,c). The ligand remained bound to the active site for only 15-

30% of the simulation time, despite its initial placement inside the ligand-binding pocket. The analysis of electrostatic surface potential revealed the presence of a large, negatively charged area around the substrate-binding pocket of ARG1 that likely plays a role in attracting positively charged L-arginine to the catalytic site (Fig. 4c). Since PHZ in the presence of oxygen leads to the formation of free radicals and hydrogen peroxide[21], we hypothesized that decreased ARG activity in CECs from HA-PHZ mice might emerge due to non-specific non-covalent interactions of PHZ with the catalytic pocket of ARG1 that leads to oxidative changes in the enzyme, decreased activity, and compensatory increase in its expression. Indeed, the incubation of recombinant ARG1 with PHZ in the presence of oxygen led to a significant increase in the carbonylation of the enzyme. However, this effect was only slightly reduced by concomitant incubation with N-acetylcysteine (ROSi) (Fig. 4d). Moreover, ROS scavengers did not prevent ARG1 induction by PHZ *in vivo* (Supplementary Fig. 10a,b) nor *in vitro* (Supplementary Fig. 10c,d). Thus, we demonstrated that PHZ targets ARG leading to the diminishment of CECs immunoregulatory properties, however, the exact mechanism that would explain PHZ-mediated inhibition of ARG activity remains elusive.

CECs degrade L-Arg and produce ROS leading to the suppression of T-cells

Due to the interaction between PHZ and arginases, we chose NHA as a model of anemia-induced CECs for further studies. We found that $CD4^+$ T-cells stimulated with anti-CD3/CD28 beads in the presence of CECs showed downregulation of activation markers CD25 and CD69, which was less pronounced for CD62L (Fig. 5a). Both arginase inhibitor (ARGi, OAT-1746, a membrane-permeable, potent inhibitor of both arginase isoforms[22-24]) and ROS inhibitor (ROSi, N-acetylcysteine) nearly completely

restored the proliferation of T-cells that was inhibited by co-culture with CECs isolated from NHA mice (Fig. 5b), similar to CECs isolated from neonates (Supplementary Fig. 11). Likewise, CECs-conditioned medium had a suppressive effect on T-cell proliferation, and supplementation with either of L-arginine or ARGi restored T-cell proliferation to percentages akin to the control group (Fig. 5c).

To confirm that early-stage CECs that have the highest ROS levels (Supplementary Fig. 5) and ARG expression (Supplementary Fig. 6) have the most potent suppressive effects on T-cells, we isolated the fraction of nucleated cells (erythroid progenitors, developmental stages I-III, Fig. 1i) from CECs using density gradient centrifugation. We found that the whole CECs population suppressed $CD4^+$ T-cells proliferation by 43% while isolated nucleated CECs (nCECs) completely inhibited it (Fig. 5d), confirming that they are responsible for the suppressive effects.

At a 1:10 of T-cells to CECs ratio, similar to that observed in anemia (Supplementary Fig. 3f,g), CECs completely suppressed the proliferation of $CD4^+$ (Fig. 5e) and $CD8^+$ T-cells (Fig. 5f). Further studies revealed that the expansion of CECs in anemic mice leads to the substantial increase of the total arginase activity (Fig. 5g). This effect was caused by an increased ARG2 but not ARG1 levels in the spleen (Fig. 5h-j). Even though the concentration of L-arginine was only slightly decreased in the serum of anemic mice (Supplementary Fig. 12), their splenic $CD4^+$ T-cells and $CD8^+$ T-cells had decreased levels of CD3ζ (Fig. 5k,l), a marker of L-arginine T-cell starvation[25,26]. Accordingly, *ex vivo* stimulation of T-cells with anti-CD3/CD28 beads in the presence of CECs resulted in a decrease in CD3ζ, which was prevented by ARGi and completely restored by the combination of ARGi and ROSi (Fig. 5m,n). Noteworthy, the decrease in CD3ζ was not observed in the lymph nodes of anemic mice, where CECs are a relatively rare population (Supplementary Fig. 13a-c). Altogether, these

242 results show that CECs suppress T-cells response in anemic mice *via* both arginase
243 and ROS and their local accumulation in the spleen impairs T-cell immunity.

244 To further study the role of ARG2 in the modulation of immune response by CECs,
245 we assessed the suppressive effects of CECs isolated from anemic mice lacking
246 functional *Arg2* gene (*Arg2*$^{-/-}$, *Arg2*$^{tm1Weo/}$J mice[27]). *Arg2*$^{-/-}$ mice had effective stress
247 erythropoiesis (Supplementary Fig. 14a). Despite a slightly increased percentage of
248 ARG1^{+} CECs compared to wild-type mice (*Arg2*$^{+/+}$) (Supplementary Fig. 14b), no
249 significant changes in total ARG1 levels were observed in these cells (Supplementary
250 Fig. 14c). In contrast to wild-type mice, expansion of CECs in the spleen of anemic
251 *Arg2*$^{-/-}$ mice was not associated with a significant decrease in CD3ζ in T-cells (Fig.
252 6a,b). Moreover, CECs isolated from *Arg2*$^{-/-}$ mice had substantially diminished
253 suppressive effects on T-cell proliferation as compared with *Arg2*$^{+/+}$ CECs (Fig. 6c),
254 confirming a critical role of ARG2 in the regulation of T-cells function by murine
255 CECs.

256

257 **CECs expand in the blood of anemic individuals and suppress IFN-γ**
258 **production by T-cells**

259 Then, we sought to investigate the role of CECs in anemic patients (Supplementary
260 Table 1, Supplementary Table 2). The percentages of CECs (CD71^{+}CD235a^{+}) in the
261 peripheral blood were substantially increased in anemic patients compared to non-
262 anemic control individuals (Fig. 7a,b). The number of CECs in the blood (Fig. 7c)
263 reversely correlated with hemoglobin concentration (Fig. 7d) and was the highest in
264 patients with moderate and severe anemia (Fig. 7e).

In anemic patients, CECs constituted a substantial fraction of peripheral blood mononuclear cells (PBMCs) (Fig. 7f,g) and were predominantly at the latest stages of differentiation with a very small percentage of $CD45^+$ CECs (Supplementary Fig. 15a,b). We found that the production of IFN-γ in response to CD3/CD28 stimulation was suppressed in T-cells from anemic individuals when compared to non-anemic controls (Fig. 7h, i). However, T-cells proliferation (Supplementary Fig. 15c,d) or the production of TNF-α by myeloid cells in response to killed bacteria (Supplementary Fig. 15e) were comparable in anemic patients and control individuals.

CECs from human bone marrow suppress T-cells proliferation

Since the expansion of CECs in the peripheral blood of anemic individuals was not associated with the suppression of T-cells proliferation, we investigated the immunoregulatory properties of CECs from the healthy human bone marrow (Fig. 8a). CECs in the bone marrow are enriched with early-stage CECs (Supplementary Fig. 16a,b) and are predominantly $CD45^+$ (Supplementary Fig. 16c,d). Similar to murine CECs, their counterparts in the human bone marrow express ARG2 (Fig. 8b-d). Importantly, human erythroid cells also express ARG1 (Fig. 8b-d). The expression of both ARG isoforms was higher in $CD45^+$ than in $CD45^-$ CECs (Supplementary Fig. 16e,f). CECs isolated from human bone marrow (Supplementary Fig. 16g) significantly suppressed proliferation of both $CD4^+$ and $CD8^+$ T-cells (Fig. 8e,f). These effects were diminished by the ARGi, confirming arginase-dependent effects of human CECs.

Erythroleukemia-derived erythroid cell lines suppress T-cells in an ARG- and ROS-dependent mechanism

Further, we investigated the immunoregulatory properties of model human erythroleukemia-derived erythroid cell lines: K562, HEL92.1.7, and TF-I. These cells express multiple erythroid-lineage markers, including CD71 and CD235a (Fig. 9a), and spontaneously differentiate into erythroblast-like cells. We found that similarly to primary CECs, erythroid cells have substantial arginase activity (Supplementary Fig. 17a), express both ARG1 (Supplementary Fig. 17b) and ARG2 (Supplementary Fig. 17c), and have high ROS levels (Supplementary Fig. 17d). Notably, all examined types of erythroid cells potently suppressed proliferation of human $CD4^+$ (Fig. 9b-e) and $CD8^+$ (Fig. 9f-i) T-cells in an ARG- and ROS-dependent manner (Fig. 9e,i, Supplementary Fig. 18a,b).

Suppression of T-cells function is a general feature of erythroid cells which disappears during their maturation

Our results demonstrated that T-cell suppression is a common feature of both murine and human CECs. Apparently the immunoregulatory properties were the most potent at the earliest stages of differentiation when the levels of ROS, ARG1, and ARG2 are the highest. Therefore, we next sought to establish a model of *ex vivo* differentiation of erythroid cells. To this end, CECs were expanded and differentiated from PBMCs of healthy human donors (Supplementary Fig. 19a). PBMC-derived CECs expressed erythroid markers, including CD71, CD235a, CD36, and CD49d, and had high expression of CD44 and CD45 (Supplementary Fig. 19a,b). Similar to their bone marrow counterparts, PBMCs-derived CECs had high levels of both ARG1 and

ARG2 (Supplementary Fig. 20a,b). Moreover, isolated PBMC-derived CECs (Fig. 10a) potently suppressed both $CD4^+$ and $CD8^+$ human T-cell proliferation (Fig. 10b,c).

Next, we aimed to study the possible changes in immunoregulatory properties of erythroid cells during differentiation into RBC. First, we investigated whether hematopoietic stem and progenitor cells (HSPCs) exert immunosuppressive effects. Mobilized hematopoietic stem cells obtained from peripheral blood (peripheral blood stem cells, PBSCs, Supplementary Fig. 21a) had high ARG1 and ARG2 levels (Supplementary Fig. 21b) and included only a small percentage of CECs (Supplementary Fig. 21c). Despite high arginase expression, peripheral blood stem cells had no impact on T-cell proliferation (Supplementary Fig. 21d,e).

Then, using continuous CECs culture, we demonstrated that CECs differentiated from PBMCs (Fig. 10d) exert robust, but transient suppressive properties, that disappear during erythroid differentiation (Fig. 10e-g). We found that of all CECs developmental stages, cells at the stage of $CD71^{high}$ $CD235a^{mid}$ most strongly inhibited T-cells proliferation (Fig. 10f,g). Moreover, these cells potently suppressed T-cells activation based on the CD25 and CD69 levels (Supplementary Fig. 22a,b) as well as inhibited IFN-γ production by T-cells (Supplementary Fig. 22c). The suppression depended on both ARG and ROS since only the combination of ARGi and ROSi significantly diminished suppressed T-cell activation, IFN-γ production (Supplementary Fig. 22c), and proliferation (Supplementary Fig. 23a,b). Loss of the suppressive properties corresponded with a decrease in CD71 (Fig. 10h), an increase in CD235a (Fig. 10i) as well as a decrease in CD49d (Fig. 10k) levels, the latter being a marker of the transition to the reticulocyte stage[28,29]. Subsequent CECs differentiation resulted in a complete loss of suppressive effects on T-cells.

Further, we observed that induction of erythroid differentiation of K562 cells by sodium butyrate[30] (Supplementary Fig. 24a) was associated with a decrease of immunosuppressive effects on T-cells (Supplementary Fig. 24b). These differentiated cells had decreased ARG2, but not ARG1 levels (Supplementary Fig. 24c), and decreased total arginase activity as compared with non-differentiated K562 cells (Supplementary Fig. 24d). Downregulation of ARG2 was most probably caused by mitophagy, a crucial process during erythroid differentiation[31], as evidenced by the decreased signal from a mitochondrial probe in differentiated K562-erythroid cells (Supplementary Fig. 24e). Similar changes in ARG expression were also detected in primary murine (Supplementary Figure 6b-e) and human CECs (Supplementary Figure 20b). Finally, we demonstrated that mature RBCs obtained from healthy donors had no impact on T-cell proliferation (Supplementary Fig. 25a-c). Altogether, we show that human CECs possess robust, but transient suppressive properties that are most potent in the earliest developmental stages and disappear during erythroid cell maturation.

Discussion

In this study, we demonstrate that suppression of T-cells is a general feature of murine and human CECs. Anemic CECs *via* arginases and ROS suppress proliferation and production of IFN-γ by T-cells. Using continuous human erythroid cell culture, we show that the immunoregulatory properties of CECs are transient and disappear during maturation.

Recent studies have broadened our understanding of the many roles played by CECs expanded by different triggers[3]. Immunoregulatory functions of CECs were

reported for the first time in neonates that are characterized by a physiological abundance of CECs[4]. Neonatal CECs suppress anti-bacterial immunity *via* ARG2 by decreasing the production of proinflammatory cytokines by myeloid cells[4] and by suppressing antibody production in response to *B. pertussis*[6]. We found that in adult mice anemia induced the expansion of early-stage CECs that had the highest expression of ARG2. Neither ARG2-expressing CECs nor recombinant ARG1 suppressed the production of TNF-α from myeloid cells. However, arginases seem to primarily impair T-cells by decreasing their activation and proliferation[32]. Accordingly, we observed decreased proliferation of adoptively transferred OT-I cells in the spleen of anemic mice, which was reflected *ex vivo* in the co-culture of murine T-cells with CECs. Expansion of CECs in the spleen of anemic mice resulted in the increased ARG activity in the spleen leading to the L-arginine starvation of T-cells, decreased levels of CD3ζ, and suppressed proliferation. Moreover, human CECs expressed both ARG1 and ARG2 and suppressed T-cell proliferation in an ARG-dependent manner. Thus, expansion of ARG-expressing CECs in anemia may induce immune suppression, similar to the expansion of ARG-expressing myeloid cells in cancer[33] and during pregnancy[34].

CECs were also reported to modulate immune response *via* ROS in tumor-bearing mice and cancer patients[10]. We found that ROSi restored T-cell proliferation in co-culture with CECs from anemic mice to a similar extend as ARGi. Importantly, ROS also may decrease CD3ζ in T-cells[35]. However, ROSi restored CD3ζ decreased by CECs only in combination with ARGi, which confirms that ARG cooperates with ROS in CECs to induce T-cells hyporesponsiveness to proliferative triggers.

Importantly, we demonstrated that previously described lack of immunosuppressive capacities of CECs in anemic mice[10] resulted from the

386 interaction between PHZ used to induced anemia and ARGs. PHZ-induced hemolytic
387 anemia is one of the most commonly used models of anemia. PHZ leads to the
388 formation of ferrihemoglobin from oxyhemoglobin and production of free radicals that
389 disrupt the interactions between hem and globin chains leading to the formation of
390 Heinz bodies and hemolysis[21]. However, PHZ-induced CECs are less effective in
391 suppressing T-cell proliferation as compared with CECs isolated from neonatal or
392 other anemic mice. We show that PHZ targets ARGs, critical immunomodulating
393 enzymes. It needs to be considered in future studies that the interaction between
394 PHZ and ARGs may have considerable effects on the obtained results.

395 Anemia correlates with worse outcomes in many diseases, including
396 pneumonia[36] or cancer[37]. Moreover, preoperative anemia is associated with an
397 increased risk of infection and mortality in patients undergoing surgery[38,39]. We
398 demonstrated that CECs expand in anemic patients and may suppress the
399 production of cytokines by T-cells. A small fraction of $CD45^+$ CECs in the peripheral
400 blood of our cohort subject is consistent with a recent report on CECs in systemic
401 juvenile idiopathic arthritis patients[40]. In line with our results, a recent study showed
402 that anemia status influences the blood transcriptome with enrichment of erythrocyte
403 differentiation genes as well as ARG1 in anemic children, but decreased signatures
404 of $CD4^+$ T-cell activation and differentiation[41]. It remains unknown to which extent
405 CECs are responsible for immune suppression and whether in these conditions
406 supplementation of iron, vitamin B12, or administration of erythropoiesis-stimulating
407 agents including EPO may restore immune response.

408 Erythropoiesis is a continuum of developmental states that gives mature red
409 blood cells from a hematopoietic stem cell (HSC) and is strictly regulated by multiple
410 factors[42]. Recent studies demonstrated that immunomodulatory properties are strong

411 in early-stage CD45^{+} CECs in contrast to more mature CD45^{-} CECs that lack these
412 capacities[9,10,17,43]. However, other studies also reported the immunomodulatory role
413 of CD45^{-} CECs[40,44], which suggests that CD45 alone may not be a reliable marker of
414 immunosuppressive CECs. Here, we showed that human CECs acquire
415 immunomodulatory properties during erythroid differentiation and are the most potent
416 in an early stage characterized by the CD71^{high} CD235a^{mid} phenotype. Further
417 erythroid maturation is associated with the disappearance of the suppressive
418 properties. These early-stage CECs are relatively rare in the peripheral blood of
419 anemic individuals, which may be a reason for the lack of T-cell proliferation
420 suppression. In contrast, human bone marrow is enriched in early-stage CECs that
421 suppress T-cells proliferation. Nonetheless, the suppression of T-cells by bone
422 marrow CECs was substantially weaker than that of CD71^{high} CD235a^{mid} CECs from
423 *ex vivo* culture. This may be explained by the fact that in human bone marrow CECs
424 at the earliest stages of differentiation are still much less abundant than late-stage
425 CECs[28,45].

426 The exact role of transient immunomodulatory properties of CECs remains
427 elusive. It was suggested that expansion of CECs in neonates provides tolerance to
428 harmless antigens, including the commensal microbiota[4], and minimalize damage
429 caused by inflammation in the intestines[4], liver[7], and lungs[46] during the first days of
430 postnatal life. In adults, the role of CECs seems to be similar. Recent studies
431 demonstrated that stress erythropoiesis is a key inflammatory response[47], therefore,
432 expansion of CECs may prevent progression to chronic inflammation. Indeed,
433 transfer of CECs suppressed inflammatory response and attenuated the wasting
434 syndrome in murine models of colitis[11]. In cancer, which is characterized by a chronic
435 inflammation[48], CECs substantially expand and suppress immune response

436 facilitating tumor growth and increasing the susceptibility to pathogens[10]. On the
437 other hand, impaired immunoregulatory properties of CECs may exacerbate the
438 damage caused by inflammation[49]. Moreover, CECs by suppressing production of
439 IFN-γ, a crucial inflammatory cytokine and a potent inhibitor of erythropoiesis[50,51],
440 may allow maintenance of erythropoiesis and play a role in preventing systemic
441 inflammation.

442 Importantly, most of the knowledge on CECs has been build based on murine
443 models[5]. However, several crucial divergences between mice and humans may limit
444 the translational character of CECs studies in mice, that include differences in stress
445 erythropoiesis[52]. In mice, stress erythropoiesis primarily takes place in the spleen and
446 relies on the expansion of early-stage CECs[53]. Thus, suppressive CECs may interact
447 with immune cells in the spleen, which is also an active immune organ[54]. We
448 observed that T-cells in anemic mice are rather locally suppressed in the spleen,
449 while not affected in the lymph nodes, similar to the conditions described for
450 neonates[4]. In contrast, in humans stress erythropoiesis primarily involves the bone
451 marrow, and expansion of CECs in extramedullary sites is rather occasional[5,52].
452 Moreover, CECs at the earliest stages of differentiation are relatively rare in healthy
453 individuals[45]. Thus, it seems that CECs may have the most significant
454 immunoregulatory role under conditions that are characterized by the impaired
455 erythroid differentiation and robust enrichment of early-stage CECs, that include
456 cancer[55].

457 Our findings might be of relevance in better understanding the mechanisms
458 underlying suppressed cell-mediated immunity and anti-bactericidal capacity of
459 leucocytes[56] and the impaired of T-cell mediated immunity in anemic children[57].

460 Moreover, our study suggests that CECs may be a crucial regulator of immune
461 response in different disease conditions.

Methods

Reagents

Recombinant human ARG1 was obtained from Biolegend (San Diego, CA, USA), recombinant murine Arg1 was obtained from Cloud-Clone Corp., arginase inhibitor OAT-1746 was synthesized at OncoArendi Therapeutics, Warsaw, Poland. All other reagents, if not otherwise stated, were obtained from SigmaAldrich.

Cell lines

K562, HEL92.1.7 and TF-I cell lines were purchased from American Type Culture Collection (ATCC). Cells were cultured in RPMI-1640 medium supplemented with 10% heat-inactivated fetal bovine serum (FBS, HyClone), 2 mM L-glutamine (SigmaAldrich) 100 U/ml penicillin and 100 µg/ml streptomycin (SigmaAldrich) at 37°C in a humidified atmosphere of 5% CO_2 in the air. Additionally, TF-I cells medium contained 2 ng/ml of recombinant human GM-CSF (R&D Systems). Cells have been cultured for no longer than 4 weeks after thawing and were regularly tested for *Mycoplasma* contamination using PCR technique and were confirmed to be negative.

Human samples

Human PBMCs used as a source of $CD4^+$ and $CD8^+$ T-cells and used for the expansion and differentiation of PBMC-derived CECs were isolated from buffy coats obtained commercially from the Regional Blood Centre in Warsaw, Poland. PBMCs were isolated by density gradient centrifugation method using Histopaque®-1077 (SigmaAldrich) or Lymphoprep™ (STEMCELL Technologies), according to the manufacturer's protocols. All donors were males between the ages of 18 and 45 years old. Donors were screened for general health and qualified by the physician for

blood donation. All donors had negative clinical laboratory tests for HIV-1, HIV2, hepatitis B, and hepatitis C and hematology values within normal ranges.

Peripheral blood samples were obtained from patients hospitalized in the Central Teaching Clinical Hospital, Medical University of Warsaw or treated in the Outpatient Clinic of Central Teaching Clinical Hospital, Medical University of Warsaw, Warsaw. The study was conducted in accordance with the Declaration of Helsinki. The study was approved by the Bioethical Committee of the Medical University of Warsaw (KB/8/2021). Patients with or without anemia based on WHO diagnostic criteria[58] were enrolled in the study. Patients with proliferative diseases, including cancer, were excluded. The blood samples were obtained by venipuncture and subjected to complete blood count evaluation. The remaining blood was used for further examination. Flow cytometry was performed as described below. CountBright™ Absolute Counting Beads (Thermo Fisher Scientific) were used for CECs counting. PBMCs were purified from whole blood of anemic and non-anemic patients by density separation using Lymphoprep (STEMCELL Technologies).

Human bone marrow samples were commercially obtained from Lonza Walkersville, Inc. Aspirates were withdrawn from bilateral punctures of the posterior iliac crests. Every 100 ml of bone marrow was collected into syringes containing 10 ml of heparin (Porcine Intestinal Mucosa) Sodium Injection (~100 units heparin per ml bone marrow). Bone marrow samples were obtained from both healthy males (n=6) and healthy non-pregnant females (n=3) US-based donors between the ages of 23 and 45 years old. Samples were collected after obtaining permission for their use in research applications by informed consent or legal authorization. All donors were screened for general health and negative medical history for heart disease, kidney

disease, liver disease, cancer, epilepsy, and blood or bleeding disorders. All donors had negative clinical laboratory tests for HIV-1, HIV2, hepatitis B, and hepatitis C.

Mobilized peripheral blood stem cells (PBSCs) were obtained from familial donors from the material remaining after allogeneic stem cell transplantation. PBSCs were mobilized with the granulocyte colony-stimulating factor (G-CSF) and isolated from the donor peripheral blood using apheresis according to the standard clinical protocol. Informed consent was obtained from PBSCs donors. Collected PBSCs were subjected to density gradient centrifugation using Lymphoprep (STEMCELL Technologies) to remove dead cells and debris, washed three times with RPMI medium, and used for the analysis.

Mice

Wild-type C57BL/6 mice, both male and female, 8 to 14-week-old were obtained from the Animal House of the Polish Academy of Sciences, Medical Research Institute (Warsaw, Poland). Transgenic mice of C57BL/6 genetic background, B6.129S4-Arg1^{tm1Lky}/J (YARG Mice co-expressing Arg1 and enhanced yellow fluorescent protein (eYFP)[59], stock #015857), C57BL/6-Tg(TcraTcrb) 1100Mjb/J (OT-I, TCR transgenic mice producing OVA peptide-specific CD8$^+$ T cells[60], stock #003831) and Arg2^{tm1Weo}/J (Arg2$^{-/-}$, Arg2 functional knockout[27]), were purchased from the Jackson Laboratories and bred at the animal facility of the Department of Immunology, Medical University of Warsaw. Mice were housed in controlled environmental conditions in specific-pathogen-free (SPF) conditions (breeding cages, OT-I mice) or conventional (others) animal facility of the Department of Immunology, Medical University of Warsaw, with water and food provided ad libitum. For mice genotyping, DNA was isolated with DNeasy Blood & Tissue Kit (QIAGEN) according to the

manufacturer's instructions. The concentration and purity of DNA were determined using the NanoDrop 2000c spectrophotometer (Thermo Fisher Scientific). PCR reaction was performed using OneTaq® 2× Master Mix with Standard Buffer (New England Biolabs). Primers sequences, PCR, and agarose electrophoresis conditions were set according to genotyping protocols available on The Jackson Laboratory website (https://www.jax.org). The experiments were performed in accordance with the guidelines approved by the II Local Ethics Committee in Warsaw (approval No. WAW2/117/2019 and WAW2/143/2020) and in accordance with the requirements of the EU (Directive 2010/63/EU) and Polish (Dz. U. poz. 266/15.01.2015) legislation.

Animal anemia models

To induce non-hemolytic anemia (NHA) mice were phlebotomized 4 and 2 days before harvest. At least 100 µl of blood was collected each time. To induce hemolytic anemia (HA), mice were injected intraperitoneally (i.p.) three days before harvest with 50 mg per kg body weight of phenylhydrazine (PHZ) hydrochloride solution (HA-PHZ) or mice were injected intravenously (i.v.) six days before harvest with 45 µg of anti-TER119 monoclonal antibody (TER-119, BioXCell) into the caudal vein. For the analysis of stress erythropoiesis, mice were injected i.v. with 30 µg of anti-TER119 monoclonal antibody (TER-119, BioXCell) into caudal vein followed by the monitoring of RBC count in the peripheral blood. For complete blood count, blood was collected into EDTA-coated tubes from inferior palpebral veins and examined using Sysmex XN-2000 Hematology Analyzer. The parameters of complete blood counts and reference intervals[61] are presented in Supplementary Fig. 1. For the analysis of amino acid concentration, blood was collected into IMPROMINI® Gel & Clot Activator Tubes. Tubes were gently inverted five times to mix the clot activator and incubated

for 30 min at room temperature (RT) followed by centrifugation for 10 min at 1000 x g at 4°C. Serum was collected and stored at -20°C until analysis. L-arg concentration in the serum was determined with ultra-performance liquid chromatography-tandem mass spectrometry (UPLC-MS/MS) method on Waters Xevo TQ-S mass spectrometer equipped with Waters Acquity UPLC chromatograph (Waters) in the Mass Spectrometry Lab at the Institute of Biochemistry and Biophysics, Polish Academy of Sciences, Warsaw, Poland.

Antibodies

Fluorophore- or biotin-conjugated antibodies specific for mouse cell-surface antigens and cytokines were as follows: anti-CD71 (8D3, NovusBio; R17217, eBioscience), anti-TER119 (TER-119, BioLegend), anti-CD45.2 (104, BD Biosciences), anti-CD45 (30-F11, BioLegend), anti-CD44 (IM7, BioLegend), anti-CD3e (145-2C11, eBioscience), anti-CD4 (GK1.5, eBioscience; RM4-5. eBioscience), anti-CD8a (53-6.7, eBioscience), anti-CD69 (H1.2F4, eBioscience), anti-CD25 (PC61.5, eBioscience), anti-CD62L (MEL-14, Invitrogen), anti-CD11b (M1/70, BioLegend), anti-CD11c (HL3, BD Bioscience), anti-CD3 zeta (H146-968, Abcam), anti-IFN-γ (XMG1.2, eBioscience), anti-TNF-α (MP6-XT22, eBioscience), anti-Arg1 (polyclonal, IC5868P/F, R&D Systems), anti-Arg2 (ab81505, Abcam), goat anti-rabbit IgG (Invitrogen).

Fluorophore- or biotin-conjugated antibodies specific for human cell-surface antigens and cytokines were as follows: anti-CD71 (CY1G4, BioLegend, DF1513, NovusBio), anti-CD235a (HI264, BioLegend), anti-CD44 (IM7, BioLegend), anti-CD25 (BC96, eBioscience), anti-CD69 (FN50, e Bioscience), anti-CD45 (HI30, BD Bioscience), anti-CD49d (9F10, eBioscience), anti-CD36 (NL07, eBioscience), anti-CD34 (561,

586 BioLegend), anti-CD3 (OKT3, eBioscience), anti-CD4 (RPA-T4, eBioscience), anti-
587 CD8a (RPA-T8, eBioscience), anti-IFN-γ (4S.B3, BioLegend), anti-TNF-α (MAb11,
588 BD Bioscience), anti-Arg1 (polyclonal, IC5868P/F, R&D Systems), anti-Arg2
589 (ab137069, Abcam), goat anti-rabbit IgG (Invitrogen).

590

591 **Flow cytometry analysis**

592 Flow cytometry was performed on FACSCanto II (BD Biosciences) or Fortessa X20
593 (BD Biosciences) operated by FACSDiva software. For data analysis Flow Jo v10.6.1
594 software (TreeStar) or BD FACSDiva software (BD Biosciences) were used. Murine
595 whole blood was collected from the inferior palpebral vein to EDTA-coated tubes.
596 Spleens were isolated from mice and mechanically dispersed by pressing gently
597 through a 70 µm nylon cell strainer using a rubberized 1 ml syringe piston. Murine
598 bone marrow was isolated from the femur by the centrifugation method. Briefly,
599 femurs were dissected, followed by the removal of any muscle or connective tissue.
600 The condyles and epiphysis were removed and a cleared bone was placed in
601 microcentrifuge tubes followed by centrifugation at 2500 x g for 30 sec. Bone marrow
602 cells were filtered through a 70 µm nylon strainer and used for further analysis. No
603 erythrocyte lysis was performed in flow cytometry analysis or experiments that
604 involved analysis or isolation of CECs or RBCs. If only other types of cells were
605 analyzed using flow cytometry, erythrocytes were lysed using ACK (Ammonium-
606 Chloride-Potassium) Lysing Buffer (Thermo Fisher Scientific), according to the
607 manufacturer's protocol.

608 For cell surface staining, cells were stained with Zombie NIR™, Zombie UV™ or
609 Zombie Aqua™ Fixable Viability Kit (BioLegend), blocked on ice with 5% normal rat
610 serum in FACS buffer (PBS; 1% BSA, 0.01% sodium azide), and then incubated for

30 min on ice with fluorochrome-labeled antibodies. Fluorochrome-conjugated antibodies used for the staining are listed above. After washing in FACS buffer, cells were immediately analyzed.

For nucleus staining, cells were incubated before cell surface staining with Hoechst 33342 Fluorescent Stain (Invitrogen) at a final concentration of 1 µg/ml in Dulbecco's phosphate-buffered saline (DPBS) for 30 min, followed by a wash in DPBS. For mitochondrial staining, cells were incubated before cell surface staining with MitoSpy™ Red CMXRos (BioLegend) at a final concentration of 50 nM in RPMI medium at 37°C for 30 min, followed by a wash in FACS buffer.

For intracellular staining, membrane-stained cells were fixed using Fixation Buffer for 30 min at RT, followed by a wash with permeabilization buffer, and staining with an antibody diluted in permeabilization buffer for 30 min at RT (Intracellular Fixation & Permeabilization Buffer Set, eBioscience). For anti-ARG2 indirect intracellular staining, cells were fixed using Fixation Buffer for 30 min at RT, followed by a wash with permeabilization buffer, and staining with anti-ARG2 antibody for 1 h at RT, followed by a wash with permeabilization buffer and staining with fluorochrome-conjugated goat anti-rabbit IgG for 30 min at RT. Gating strategies used to analyze the flow cytometry data are presented in Supplementary Figures 26-44.

IFN-γ and TNF-α production assay of murine cells

Murine splenocytes were isolated from anemic or healthy mice. Cells were plated in round-bottomed 96-well plates (1×10^6 cell per well) in L-arginine-free RPMI-medium (SILAC RPMI-medium, Thermo Fisher Scientific) supplemented with 10% dialyzed FBS (Thermo Fisher Scientific), 2 mM glutamine, 100 U/ml penicillin, 100 µg/ml

streptomycin, 40 mg/L L-lysine, and 150 µM L-arginine (all from Sigma-Aldrich). Splenocytes were stimulated with Heat Killed *E. coli 0111:B4* (HKEc, InvivoGen) at the concentration 1×10^6 cells per ml or Dynabeads Mouse T-Activator CD3/CD28 (ratio 1:2, Thermo Fisher Scientific) in the presence of protein transport inhibitor (BD GolgiStop™) for 6 hours. Then, cells were stained with cell surface antigens-binding antibodies, followed by fixation, permeabilization, and intracellular staining for IFN-γ and TNF-α. Flow cytometry was performed on Fortessa X20 (BD Biosciences). Cell viability after culture in the presence of protein transport inhibitor was >80%.

IFN-γ and TNF-α production assay of human cells

Human PBMCs were isolated from the peripheral blood of anemic or non-anemic patients. Cells were plated in round-bottomed 96-well plates (1×10^6 cell per well) in L-arginine-free RPMI-medium (SILAC RPMI-medium, Thermo Fisher Scientific) supplemented with 10% dialyzed FBS (Thermo Fisher Scientific), 2 mM glutamine, 100 U/ml penicillin, 100 µg/ml streptomycin, 40 mg/L L-lysine, and 150 µM L-arginine (all from Sigma-Aldrich). PBMCs were stimulated with Heat Killed *E. coli 0111:B4* (HKEc, InvivoGen) at the concentration 1×10^6 cells per ml for TNF-α assessment in myeloid cells or Dynabeads Human T-Activator CD3/CD28 (ratio 1:2, Thermo Fisher Scientific) for IFN-γ assessment in T-cells in the presence of protein transport inhibitor (BD GolgiStop™) for 12 hours. Then, cells were stained with cell surface antigens-binding antibodies, followed by fixation, permeabilization, and intracellular staining for IFN-γ and TNF-α. Flow cytometry was performed on Fortessa X20 (BD Biosciences). Cell viability after culture in the presence of protein transport inhibitor was >93%.

For the analysis of the effect of PBMC-derived CECs on T-cells activation and IFN-γ production, PBMCs were isolated from the peripheral blood healthy blood donor. $CD4^+$ or $CD8^+$ T-Cells were isolated from PBMC using EasySep™ Human $CD4^+$ or $CD8^+$ T-Cell Isolation Kit (STEMCELL Technologies) according to the manufacturer's protocols. $CD4^+$ or $CD8^+$ T-Cells were plated in round-bottomed 96-well plates (2×10^4 cell per well) in L-arginine-free RPMI-medium (SILAC RPMI-medium, Thermo Fisher Scientific) supplemented with 10% dialyzed FBS (Thermo Fisher Scientific), 2 mM glutamine, 100 U/ml penicillin, 100 µg/ml streptomycin, 40 mg/L L-lysine, and 150 µM L-arginine (all from Sigma-Aldrich). T-cells were stimulated with Dynabeads Human T-Activator CD3/CD28 (ratio 1:2, Thermo Fisher Scientific) in the presence of PBMC-derived CECs (ratio 1:2, 4×10^5 CECs per well). The arginase inhibitor OAT-1746 (1500 nM), or N-acetylcysteine (200 µM) were added as indicated in the figures. In these concentrations, ARGi and ROSi had no effects on T-cells nor CECs viability. Human T-cells were incubated for 72 h at 37°C in 5% CO_2. Protein transport inhibitor (BD GolgiStop™) was added for the last 12 hours. Then, cells were stained with cell surface antigens-binding antibodies, followed by fixation, permeabilization, and intracellular staining for IFN-γ and TNF-α. Flow cytometry was performed on Fortessa X20 (BD Biosciences). Cell viability after culture in the presence of protein transport inhibitor was >86%.

In vivo OVA immunization and analysis of the humoral response

Control and NHA mice were immunized with albumin from chicken egg white (OVA, Ovalbumin) from Sigma (Grade VII). Each mouse received 25 µg of OVA with Imject™ Alum Adjuvant (ALUM, Thermo Fisher Scientific) at a ratio of 1:1 in the final volume of 100 µl per mouse administered i.p. After 14 days, mice were challenged

once again with the same dose of OVA-ALUM. NHA mice were divided into three groups. NHA before mice were phlebotomized before first immunization, NHA boost mice were phlebotomized before second OVA immunization, and NHA both were phlebotomized before first and second immunization (see Supplementary Fig. 3c). Untreated mice received Imject™ Alum Adjuvant without OVA. Blood was obtained from mice 14 days after the second immunization, plasma was isolated and stored at -80ºC. The concentration of anti-OVA IgG antibodies was determined using Anti-Ovalbumin IgG1 (mouse) ELISA Kit (Cayman Chemical).

***In vivo* proliferation assay**

OVA (SIINFEKL)-specific $CD8^+$ T cells were isolated from the spleen and lymph nodes of healthy 6-8-week old OT-I mice using EasySep™ Mouse $CD8^+$ T-Cell Isolation Kit (STEMCELL Technologies) according to the manufacturer's protocols. Isolated OT-I cells labeled with CTV for 20 min at 37°C at a final concentration of 2.5 µM in PBS, washed and transferred into the caudal tail vein of host C57BL/6 mice at a cell number of 7×10^6 in 150 µl of PBS. Twenty-four hours post OT-I T-cells inoculation, host mice were challenged with 7.5 µg of full-length OVA protein (grade V, Sigma Aldrich) injected into the caudal tail vein. Three mice from controls were injected only with PBS (negative control). On day 3 post OVA immunization, spleens were harvested, mashed through a 70 µm nylon strainer, stained with OVA-specific MHC tetramers (iTAg Tetramer/PE-H-2 K^b OVA (SIINFEKL), MBL Inc., WA, USA) to detect OT-I $CD8^+$ T-cells, followed by anti-CD3 and anti-CD8 staining, and analyzed for proliferation by flow cytometry. The gate for proliferating cells (CTV^{low}) was set using unstimulated negative control. OT-I T-cells with lower fluorescence of CTV than non-proliferating T-cells were identified as proliferating cells.

709

710 **Murine T-cell proliferation assay**

711 Murine T-cells were isolated from spleens of healthy 6-8-week old C57BL/6 mice
712 using EasySep™ Mouse $CD4^+$ or $CD8^+$ T-Cell Isolation Kit (STEMCELL
713 Technologies) according to the manufacturer's protocols. CECs were isolated from
714 the spleens of anemic mice using the EasySep™ Release Mouse Biotin Positive
715 Selection Kit (STEMCELL Technologies) according to the manufacturer's protocols.
716 Biotin-conjugated anti-CD71 antibodies (anti-mouse clone 8D3, NovusBio,) were
717 used at a final concentration of 1 µg/ml. CECs purity was >80%. For cell proliferation
718 assay, T-cells were labeled with Cell Trace Violet (CTV) dye (Thermo Fisher
719 Scientific) for 20 min at 37°C at a final concentration of 2.5 µM in PBS. Next, the
720 labeled T-cells were plated in round-bottomed 96-well plates (5×10^4 cell per well) in
721 L-arginine-free RPMI-medium (SILAC RPMI-medium, Thermo Fisher Scientific)
722 supplemented with 10% (v/v) dialyzed FBS (Thermo Fisher Scientific), 2 mM
723 glutamine, 100 U/ml penicillin, 100 µg/ml streptomycin, 1% (v/v) MEM non-essential
724 amino acids solution (Thermo Fisher Scientific), 50 µM 2-Mercaptoethanol
725 (Thermofisher Scientific), and 150 µM L-arginine and 40 mg/L L-lysine (SigmaAldrich).
726 Proliferation was triggered by the stimulation with Dynabeads Mouse T-Activator
727 CD3/CD28 (ratio 1:2, Thermo Fisher Scientific). The arginase inhibitor OAT-1746
728 (ARGi, 500 nM), L-arginine (1000 µM), or N-acetylcysteine (ROSi, 100 µM) were
729 added as indicated in the figures. In these concentrations, ARGi and ROSi had no
730 effects on T-cells nor CECs viability. Murine CECs were added to the wells in a 1:2
731 ratio (1×10^5 CECs per well). Murine T-cells were incubated for 72 h at 37°C in 5%
732 CO_2. Then, cells were harvested, stained with live/dead Zombie dye (Biolegend),
733 anti-CD3 and anti-CD4 or anti-CD8 antibody, and analyzed by flow cytometry. The

gate for proliferating cells was set based on the unstimulated controls. Cell autofluorescence was determined using CTV-unstained controls. Percentages of proliferating cells were calculated using the FlowJo Software v10.6.1 (Tree Star).

Human T-cell proliferation assay

Human T-cells were isolated from peripheral blood mononuclear cells (PBMC) isolated from buffy coats commercially obtained from the Regional Blood Centre in Warsaw, Poland using EasySep™ Human $CD4^+$ or $CD8^+$ T-Cell Isolation Kit (STEMCELL Technologies) according to the manufacturer's protocols. CECs were isolated from human bone marrow aspirates or PBMC derived CECs culture using EasySep™ Release Mouse Biotin Positive Selection Kit (STEMCELL Technologies) according to the manufacturer's protocols. Biotin-conjugated anti-CD71 antibodies (anti-human clone DF1513, NovusBio) were used at a final concentration of 1 µg/ml. CECs purity was >80%. For cell proliferation assay, T-cells were labeled with Cell Trace Violet (CTV) dye (Thermo Fisher Scientific) for 20 min at 37°C at a final concentration of 2.5 µM in PBS. Next, the labeled T-cells were plated in round-bottomed 96-well plates (2×10^4 cell per well) in L-arginine-free RPMI-medium (SILAC RPMI-medium, Thermo Fisher Scientific) supplemented with 10% (v/v) dialyzed FBS (Thermo Fisher Scientific), 2 mM glutamine, 100 U/ml penicillin, 100 µg/ml streptomycin, 1% (v/v) MEM non-essential amino acids solution (Thermo Fisher Scientific), 50 µM 2-Mercaptoethanol (Thermo Fisher Scientific), and 150 µM L-arginine and 40 mg/L L-lysine (SigmaAldrich). Proliferation was triggered by the stimulation with Dynabeads Human T-Activator CD3/CD28 (ratio 1:2, Thermo Fisher Scientific). The arginase inhibitor OAT-1746 (1500 nM), or N-acetylcysteine (200 µM) were added as indicated in the figures. In these concentrations, ARGi and ROSi had

no effects on T-cells nor CECs viability. Human CECs were added to the wells in a 1:2 ratio (4×10^5 CECs per well). T-cells were incubated for 120 h at 37°C in 5% CO_2. Then, cells were harvested, stained with live/dead Zombie dye (Biolegend), anti-CD3 and anti-CD4 or anti-CD8 antibody, and analyzed by flow cytometry. The gate for proliferating cells was set based on the unstimulated controls. Cell autofluorescence was determined using CTV-unstained controls. Percentages of proliferating cells were calculated using the FlowJo Software v10.6.1 (Tree Star).

CECs-conditioned medium (CM)

Conditioned medium was obtained by culturing CECs in the arginine-free RPMI-medium (SILAC RPMI-medium, Thermo Fisher Scientific) supplemented with 150 µM L-arginine at the density 1×10^6 cells/ml for 24h. Cells were centrifuged and the supernatant was collected and immediately frozen at -80ºC. After thawing, the supernatant was filtered through a 0.45 µm Syringe Filter (Wenk LabTec) and was used in experiments a 1:1 ratio with 150 µM L-arginine RPMI SILAC medium.

Reactive oxygen species (ROS) detection

The level of ROS in cells was determined using CellROX Green Reagent (Thermo Fisher Scientific) or 2',7'-dichlorodihydrofluorescein diacetate (DCFDA). Cells were stained with CellROX at a final concentration of 5 µM or DCFDA at a final concentration of 10 µM in pre-warmed PBS for 30 minutes at 37ºC, followed by three washes with PBS. H_2O_2-treated cells served as positive controls. For some experiments, cells stained with CellROX or DCFDA were further stained with

fluorochrome-labeled antibodies on ice. Stained cells were acquired on Fortessa X20 flow cytometer (BD Biosciences).

Arginase activity assay and Griess test

Recombinant enzymes (ARG1 and ARG2) to study ARGi were produced at OncoArendi Therapeutics in *E. coli* expression system and purified by the FPLC method. The proteins were purified by FPLC and stored at -80°C in the storage buffer containing: 20 mM Tris pH 8.0, 100 mM NaCl, 10 mM DDT and 10% glycerol. The basic assay buffer was composed of 100 mM sodium phosphate buffer, 130 mM sodium chloride, 1 mg/mL BSA, pH 7.4. The enzymatic reaction was carried out in the presence of 200 µM $MnCl_2$ (cofactor) and 10 mM or 20 mM L-arginine hydrochloride (for hARG1 or hARG2, respectively), mixed at the final volume of 25 µL. Basic developing buffer contained 50 mM boric acid, 1 M sulfuric acid, 0.03% (m/v) Brij® 35 detergent. PHZ or ABH was diluted in basic assay buffer at the volume of 50 µL. The recombinant enzyme was diluted in a basic assay buffer at the volume of 25 µL. The reaction was performed at the final volume of 100 µL. Developing mixture included freshly prepared equal volume mixture of developing solution A (4 mM o-phthaldialdehyde) and solution B (4 mM N-(1-naphthyl)ethylenediamine dihydrochloride) prepared in the basic developing buffer. The compound background wells contained each of the tested compounds and the substrate/cofactor mixture, but not the recombinant enzyme (data were excluded from the analysis when the compound background exceeded 10% of the signal obtained in the wells with enzyme). The “0% activity” background wells contained only the substrate/cofactor mixture. Following 1 h incubation at 37°C, the freshly prepared developing reagent was added (150 µL) and the colorimetric reaction was developed (12 min at RT,

gentle shaking). The absorbance, proportional to the amount of the produced urea, was measured at 515 nm using Tecan's Spark™ microplate reader. Data were normalized by referring the absorbance values to the positive control wells (100% enzyme activity). The IC_{50} value was determined by the nonlinear regression method. Arginase activity in the CECs or splenocytes lysates and cell supernatant was determined using Arginase Activity Assay (Sigma) according to the manufacturer's protocol.

To evaluate nitric oxide (NO) production as a measure of NOS (nitric oxide synthase) activity, Griess Reagent System (Promega) was used according to the manufacturer's protocol. Splenocytes or CECs were isolated from murine spleens and were cultured in non-adherent 6-well plate 1×10^6 or 5×10^5 cells per 2 ml, respectively, for 24h followed by supernatants collection and measurement of NO concentration.

Bioinformatical analysis of arginase structure

The structure and predicted binding energies for the complexes of PHZ, L-arginine and 2-amino-6-borono-2-(2-(piperidin-1-yl)ethyl)hexanoic acid with both human and mouse arginases were compared. The 3D models of mouse arginases were proposed using available structures of human arginases (pdb|4hww and pdb|4hze for ARG1 and ARG2, respectively) as templates. Both templates shared more than 87 % sequence identity with their respective target. The sequence to structure alignments between mouse arginases and selected templates were calculated with the muscle program[62]. The 3D structure was proposed with MODELLER[63]. Models quality was assessed with the Molprobity webserver[64]. Next, both human and mouse proteins were prepared for docking using the Chimera dock prep module. Molecular docking

was carried out with two programs - GOLD[65] and Surflex[66]. The active site was specified based on the position of the inhibitor present in the active site of the arginase 1 (pdb|4hww). The default parameters of both programs were used.

To assess if PHZ remains stably bound to the active site of both human arginases short molecular dynamics simulations were performed. The initial configurations of ligand-protein complexes were derived from docking results for PHZ. For the PHZ-arginase complexes the simulation included the following steps. First protein and ligand were put in a dodecahedron box with the distance between solute and a box equal to 1 nm. The 0.1 M NaCl was added to the system including neutralizing counterions. After energy minimization using the steepest descent algorithm, 100 ps NVT and NPT simulation were carried out. For this modified Berendsen thermostat was used to maintain the temperature at 310 K using and Berendsen barostat to keep the pressure at 1 atm. Positions of both protein and ligand heavy atoms remained constrained. During the following 300 ps of simulation time, the ligand's constraints were gradually removed. Finally, an unconstrained 100 ns simulation is performed in which Berendsen barostat was replaced by Parrinello-Rahman barostat. During simulation short-range nonbonded interactions were cut off at 1.4nm, with long-range electrostatics calculated using the particle mesh Ewald (PME) algorithm. Bonds were constrained using the lincs algorithm. Simulations were carried out with Gromacs[67] using the gromos54a7 force field, modified to include parameters for Mn^{2+} ion adopted from[68]. Spc model was used for water molecules. Parameters for the ligand were obtained with Automated Topology Builder (ATB)[69].

Additional analyses were performed to assess if PHZ can migrate to the arginase active site when present in solute in high concentration. For this analysis protein was put in dodecahedron box with the distance between solute and a box

857 equal to 1.5 nm in which 6 PHZ molecules were placed randomly. This corresponds
858 to 0.02 M concentration of the compound. A similar simulation setup to one described
859 above was used with exception that ligand molecules remained unconstrained
860 throughout simulation.

861

862 **Protein carbonylation assay**

863 The carbonyl content of proteins was determined in a 2,4-DNPH reaction. Five µg of
864 murine ARG1 (Cloud-System Corp) was resuspended in 400 µl of distilled water and
865 incubated with PHZ (10 µM), PHZ (10 µM) with NAC (10 mM), H_2O_2 (10 mM) or
866 water (negative control) as indicated in the Fig. 3d for 1 hour at 37ºC. Proteins were
867 precipitated with 10% TCA. The precipitates were treated with either 2N HCl alone
868 (control) or 2N HCl containing 5 mg/ml 2,4-DNPH at RT for 30 min. The resulting
869 hydrazones were precipitated in 10% TCA and then washed three times with ethanol-
870 ethyl acetate (1:1). Final precipitates were dissolved in 8 M guanidine chloride. Equal
871 amounts of proteins were separated on 4-12% SDS-polyacrylamide gel (Bio-Rad),
872 transferred onto nitrocellulose membranes (Bio-Rad) blocked with TBST [Tris-
873 buffered saline (pH 7.4) and 0.05% Tween 20] supplemented with 5% non-fat milk.
874 Anti-DNP antibodies (Life Diagnostics, Inc) at concentration 1 U/ml were used for
875 overnight incubation at 4ºC. After washing with TBST, the membranes were
876 incubated with horseradish peroxidase-coupled secondary antibodies (Jackson
877 Immunores.). The reaction was developed using SuperSignal™ West Femto
878 Maximum Sensitivity Substrate (Thermofisher Scientific) and imaged using
879 ChemiDoc Touch Gel Imaging System (Bio-Rad). Densitometry was done using
880 ImageJ software.

881

882 **RNA isolation from CECs, reverse transcription, and quantitative polymerase**
883 **chain reaction**

884 Total RNA was isolated from CECs isolated from murine spleens using RNeasy Mini
885 Kit (Qiagen). RNA was subjected to reverse transcription using the GoScript™
886 Reverse Transcriptase system (Promega). All qPCRs were performed in MicroAmp
887 Fast Optical 96 WellReaction Plates (Thermo Fisher Scientific) using
888 AppliedBiosystems 7500 Fast Real-Time PCR System with 7500Software V2.0.6
889 (Thermo Fisher Scientific). Samples were assayed in triplicates. Primers sequences
890 used in the study: ARG1 forward 5'- CTCCAAGCCAAAGTCCTTAGAG-3', reverse 5'-
891 AGGAGCTGTCATTAGGGACATC-3', ARG2 forward 5'-
892 AGGAGTGGAATATGGTCCAGC-3', reverse 5'-GGGATCATCTTGTGGGACATT-3',
893 and GAPDH forward 5'-GAAGGTGGTGAAGCAGGCATC-3', reverse 5'-
894 GCATCGAAGGTGGAAGAGTGG-3' as an endogenous control. The mean Ct values
895 of a target gene and endogenous control were used to calculate relative expression
896 using the $2^{-\Delta Ct}$ method.

897

898 **Western blot**

899 Splenocytes lysates were prepared using Cell Lysis Buffer (#9803, CellSignaling
900 Technology) supplemented with protease inhibitors (Roche) according to the
901 manufacturer's protocol. Total protein concentration was assessed using Pierce BCA
902 Protein Assay Kit (Thermo Fisher Scientific). Equal amounts of whole-cell protein
903 lysates samples were boiled in Laemmli loading buffer, separated on 4-12% SDS-
904 polyacrylamide gel (Biorad), transferred onto nitrocellulose membranes (Bio-Rad)
905 blocked with TBST [Tris-buffered saline (pH 7.4) and 0.05% Tween 20]
906 supplemented with 5% non-fat milk. Anti-Arg1 antibodies (polyclonal, GTX109242,

GeneTex) at dilution 1:2000 or anti-Arg2 antibodies (polyclonal, ab81505, Abcam) at dilution 1:1000 were used for overnight incubation at 4ºC. After washing with TBST, the membranes were incubated with horseradish peroxidase-coupled secondary antibodies (Jackson ImmunoResearch). The reaction was developed using SuperSignal™ West Femto Maximum Sensitivity Substrate (Thermofisher Scientific) and imaged using ChemiDoc Touch Gel Imaging System (Bio-Rad). After imaging, bound antibodies were removed from membranes using Restore™ PLUS Western Blot Stripping Buffer (Thermofisher Scientific), followed by blocking with TBST supplemented with 5% non-fat milk. Next, the membranes were incubated with anti-β-Actin (A5060, Santa Cruz) conjugated with peroxidase. Densitometric quantifications were done using ImageJ software.

Erythroid cells differentiation

CECs were differentiated from human peripheral blood mononuclear cells (PBMC) according to the protocol by Heshusius et al.[70] with modifications. Human PBMC were purified from buffy coats from healthy donors by density separation using Lymphoprep (STEMCELL Technologies). PBMC were seeded at 1×10^6 cells/mL in erythroid differentiation-promoting medium based on StemSpan™ Serum-Free Expansion Medium (SFEM) supplemented with human recombinant EPO (2 U/ml, Roche), human recombinant stem cell factor (25 ng/ml, R&DSystems), dexamethasone (1 µM, SigmaAldrich), human recombinant insulin (10 ng/ml, SigmaAldrich), L-Glutamine (2 mM, SigmaAldrich), iron-saturated holo-transferrin (20 µg/ml, Sigma-Aldrich), sodium pyruvate (1 mM, Gibco), MEM non-essential amino acids (1% v/v, Gibco), bovine serum albumin (0.1% m/v, SigmaAldrich), EmbryoMax Nucleosides (1% v/v, Merck), and 100 U/ml penicillin and 100 µg/ml streptomycin

(SigmaAldrich). The expansion and differentiation of CECs were assessed by flow cytometry.

Statistics and Reproducibility

Data are shown as means ± SD or means ± SEM, as indicated in the figure legends. Graphpad Prism 8.4.3 (GraphPad Software) was used for statistical analyses. Data distribution was tested using the Shapiro-Wilk test, D'Agostino & Pearson test, and Kolmogorov-Smirnov test. Statistical analyses of three or more groups were compared using one-way analysis of variance (ANOVA) or Brown-Forsythe ANOVA followed by Tukey's, Dunnett's, or Bonferroni's multiple comparisons test or Kruskal-Wallis test followed by Dunn's multiple comparisons test. Repeated measures ANOVA with Sidak's or Holm-Sidak's post-hoc tests were used to analyze the differences in paired samples. Statistical analyses of two groups were compared using unpaired *t*-test, paired *t*-test, or Mann-Whitney test. Methods of statistical analyses are defined in every figure legend. *P*-value of less than 0.05 was statistically significant. Each experiment was performed in technical duplicates or triplicates. The number of biological replicates for each experiment is mentioned in the figure legends.

Data availability

Source data underlying the graphs and charts presented in the figures are available in the Supplementary Data. Uncropped western blots are provided in the Supplementary Data file. Any remaining information can be obtained from corresponding authors upon reasonable request.

Acknowledgments

This work has been co-supported by grants iONKO (Regionalna Inicjatywa Doskonalosci) from the Polish Ministry of Science and Higher Education (J.G.), 2019/35/B/NZ6/00540 (D.N.), 2017/25/B/NZ6/01139 (J.G.), and 2016/23/B/NZ6/03463 (D.N.) from the National Science Center in Poland. D.P. and M.L. are financed by TEAM program from the Foundation for Polish Science co-financed by the European Union under the European Regional Development Fund as well as grants 2019/35/O/ST6/02484 and 2020/37/B/NZ2/03757 from the National Science Center in Poland. M.L. is funded by IDUB against COVID-19 project granted by the Warsaw University of Technology under the program Excellence Initiative: Research University (IDUB). Some elements of the figures were generated with Biorender.com.

Authorship Contributions

TM.G. designed and supervised the study, conducted the experiments, analyzed the data, and wrote the manuscript. A.S. participated in *in vivo* studies. Z.R. participated in *in vitro* experiments. M.L. and D.P. performed molecular docking and molecular dynamics simulations, K.K. performed real-time qPCR and participated in *in vitro* experiments, M.M. and O.C. collected and provided human blood samples, A.R.-L. performed analysis of murine blood, M.J. participated in *in vitro* experiments, P.P and M.M.G. carried out arginase activity assays, R.B. designed and synthesized OAT-1746, M.W. bred and provided *Arg2*$^{-/-}$ mice, A.T and G.B. collected and provided HSPCs. J.G. conceived, designed and supervised the study, provided funding and wrote the manuscript. D.N. provided funding, performed in vivo studies, designed and

supervised the study, and wrote the manuscript. All authors edited and approved the final manuscript.

Competing interests

P.P., M.M.G., and R.B. are employees of OncoArendi Therapeutics, Warsaw, Poland.

References

1 Hom, J., Dulmovits, B. M., Mohandas, N. & Blanc, L. The erythroblastic island as an emerging paradigm in the anemia of inflammation. *Immunologic Research* **63**, 75-89, doi:10.1007/s12026-015-8697-2 (2015).

2 Elahi, S. Neglected Cells: Immunomodulatory Roles of CD71+ Erythroid Cells. *Trends in Immunology* **40**, 181-185, doi:https://doi.org/10.1016/j.it.2019.01.003 (2019).

3 Shokrollah, E. & Siavash, M. Immunological consequences of extramedullary erythropoiesis: immunoregulatory functions of CD71+ erythroid cells. *Haematologica* **105**, 1478-1483, doi:10.3324/haematol.2019.243063 (2020).

4 Elahi, S. *et al.* Immunosuppressive CD71+ erythroid cells compromise neonatal host defence against infection. *Nature* **504**, 158, doi:10.1038/nature12675 (2013).

5 Grzywa, T. M., Nowis, D. & Golab, J. The role of CD71+ erythroid cells in the regulation of the immune response. *Pharmacology & Therapeutics* **228**, 107927, doi:https://doi.org/10.1016/j.pharmthera.2021.107927 (2021).

6 Namdar, A. *et al.* CD71+ erythroid suppressor cells impair adaptive immunity against Bordetella pertussis. *Scientific Reports* **7**, 7728, doi:10.1038/s41598-017-07938-7 (2017).

7 Yang, L. *et al.* Regulation of bile duct epithelial injury by hepatic CD71+ erythroid cells. *JCI Insight* **5**, doi:10.1172/jci.insight.135751 (2020).

8 Delyea, C. *et al.* CD71(+) Erythroid Suppressor Cells Promote Fetomaternal Tolerance through Arginase-2 and PDL-1. *J Immunol* **200**, 4044-4058, doi:10.4049/jimmunol.1800113 (2018).

9 Chen, J. *et al.* Intratumoral CD45+CD71+ erythroid cells induce immune tolerance and predict tumor recurrence in hepatocellular carcinoma. *Cancer Letters*, doi:https://doi.org/10.1016/j.canlet.2020.12.003 (2020).

10 Zhao, L. *et al.* Late-stage tumors induce anemia and immunosuppressive extramedullary erythroid progenitor cells. *Nature Medicine* **24**, 1536-1544, doi:10.1038/s41591-018-0205-5 (2018).

11 Shim, Y. A., Weliwitigoda, A., Campbell, T., Dosanjh, M. & Johnson, P. Splenic erythroid progenitors decrease TNFα production by macrophages and reduce systemic inflammation in a mouse model of T cell-induced colitis. *European Journal of Immunology* **n/a**, doi:https://doi.org/10.1002/eji.202048687 (2020).

12 Namdar, A. *et al.* CD71⁺ Erythroid Cells Exacerbate HIV-1 Susceptibility, Mediate trans-Infection, and Harbor Infective Viral Particles. *mBio* **10**, e02767-02719, doi:10.1128/mBio.02767-19 (2019).

13 Shahbaz, S. *et al.* Erythroid precursors and progenitors suppress adaptive immunity and get invaded by SARS-CoV-2. *Stem Cell Reports* **16**, 1165-1181, doi:https://doi.org/10.1016/j.stemcr.2021.04.001 (2021).

14 Hara, H. & Ogawa, M. Erythropoietic precursors in mice with phenylhydrazine-induced anemia. *American Journal of Hematology* **1**, 453-458, doi:https://doi.org/10.1002/ajh.2830010410 (1976).

15 Hara, H. & Ogawa, M. Erythropoietic precursors in mice under erythropoietic stimulation and suppression. *Exp Hematol* **5**, 141-148 (1977).

16 Chen, K. *et al.* Resolving the distinct stages in erythroid differentiation based on dynamic changes in membrane protein expression during erythropoiesis. *Proc Natl Acad Sci U S A* **106**, 17413-17418, doi:10.1073/pnas.0909296106 (2009).

17 Elahi, S. *et al.* CD71+ Erythroid Cells in Human Neonates Exhibit Immunosuppressive Properties and Compromise Immune Response Against Systemic Infection in Neonatal Mice. *Frontiers in Immunology* **11**, doi:10.3389/fimmu.2020.597433 (2020).

18 Rodriguez, P. C. *et al.* Arginase I production in the tumor microenvironment by mature myeloid cells inhibits T-cell receptor expression and antigen-specific T-cell responses. *Cancer research* **64**, 5839-5849, doi:10.1158/0008-5472.CAN-04-0465 (2004).

19 Modolell, M. *et al.* Local suppression of T cell responses by arginase-induced L-arginine depletion in nonhealing leishmaniasis. *PLoS Negl Trop Dis* **3**, e480-e480, doi:10.1371/journal.pntd.0000480 (2009).

20 Van Zandt, M. C. *et al.* Discovery of (R)-2-amino-6-borono-2-(2-(piperidin-1-yl)ethyl)hexanoic acid and congeners as highly potent inhibitors of human arginases I and II for treatment of myocardial reperfusion injury. *Journal of medicinal chemistry* **56**, 2568-2580, doi:10.1021/jm400014c (2013).

21 Itano, H. A., Hirota, K. & Hosokawa, K. Mechanism of induction of haemolytic anaemia by phenylhydrazine. *Nature* **256**, 665-667, doi:10.1038/256665a0 (1975).

22 Czystowska-Kuzmicz, M. *et al.* Small extracellular vesicles containing arginase-1 suppress T-cell responses and promote tumor growth in ovarian carcinoma. *Nature Communications* **10**, 3000, doi:10.1038/s41467-019-10979-3 (2019).

23 Sosnowska, A. *et al.* Inhibition of arginase modulates T-cell response in the tumor microenvironment of lung carcinoma. *OncoImmunology* **10**, 1956143, doi:10.1080/2162402X.2021.1956143 (2021).

24 Pilanc, P. *et al.* A Novel Oral Arginase 1/2 Inhibitor Enhances the Antitumor Effect of PD-1 Inhibition in Murine Experimental Gliomas by Altering the Immunosuppressive Environment. *Frontiers in Oncology* **11**, doi:10.3389/fonc.2021.703465 (2021).

25 Rodriguez, P. C. *et al.* Regulation of T cell receptor CD3zeta chain expression by L-arginine. *J Biol Chem* **277**, 21123-21129, doi:10.1074/jbc.M110675200 (2002).

26 Czystowska-Kuzmicz, M. *et al.* Small extracellular vesicles containing arginase-1 suppress T-cell responses and promote tumor growth in ovarian

carcinoma. *Nature communications* **10**, 3000, doi:10.1038/s41467-019-10979-3 (2019).

27 Shi, O., Morris, S. M., Jr., Zoghbi, H., Porter, C. W. & O'Brien, W. E. Generation of a mouse model for arginase II deficiency by targeted disruption of the arginase II gene. *Mol Cell Biol* **21**, 811-813, doi:10.1128/mcb.21.3.811-813.2001 (2001).

28 Hu, J. *et al.* Isolation and functional characterization of human erythroblasts at distinct stages: implications for understanding of normal and disordered erythropoiesis in vivo. *Blood* **121**, 3246-3253, doi:10.1182/blood-2013-01-476390 (2013).

29 Nandakumar, S. K., Ulirsch, J. C. & Sankaran, V. G. Advances in understanding erythropoiesis: evolving perspectives. *Br J Haematol* **173**, 206-218, doi:10.1111/bjh.13938 (2016).

30 Chénais, B., Molle, I., Trentesaux, C. & Jeannesson, P. Time-course of butyric acid-induced differentiation in human K562 leukemic cell line: rapid increase in γ-globin, porphobilinogen deaminase and NF-E2 mRNA levels. *Leukemia* **11**, 1575-1579, doi:10.1038/sj.leu.2400755 (1997).

31 Moras, M., Lefevre, S. D. & Ostuni, M. A. From Erythroblasts to Mature Red Blood Cells: Organelle Clearance in Mammals. *Frontiers in Physiology* **8**, doi:10.3389/fphys.2017.01076 (2017).

32 Grzywa, T. M. *et al.* Myeloid Cell-Derived Arginase in Cancer Immune Response. *Front Immunol* **11**, 938, doi:10.3389/fimmu.2020.00938 (2020).

33 Zea, A. H. *et al.* Arginase-producing myeloid suppressor cells in renal cell carcinoma patients: a mechanism of tumor evasion. *Cancer research* **65**, 3044-3048, doi:10.1158/0008-5472.Can-04-4505 (2005).

34 Köstlin, N. *et al.* Granulocytic myeloid derived suppressor cells expand in human pregnancy and modulate T-cell responses. *European Journal of Immunology* **44**, 2582-2591, doi:https://doi.org/10.1002/eji.201344200 (2014).

35 Otsuji, M., Kimura, Y., Aoe, T., Okamoto, Y. & Saito, T. Oxidative stress by tumor-derived macrophages suppresses the expression of CD3 zeta chain of T-cell receptor complex and antigen-specific T-cell responses. *Proc Natl Acad Sci U S A* **93**, 13119-13124, doi:10.1073/pnas.93.23.13119 (1996).

36 Reade, M. C., Weissfeld, L., Angus, D. C., Kellum, J. A. & Milbrandt, E. B. The prevalence of anemia and its association with 90-day mortality in hospitalized community-acquired pneumonia. *BMC Pulm Med* **10**, 15, doi:10.1186/1471-2466-10-15 (2010).

37 Liu, L. *et al.* Multiple myeloma hinders erythropoiesis and causes anaemia owing to high levels of CCL3 in the bone marrow microenvironment. *Scientific Reports* **10**, 20508, doi:10.1038/s41598-020-77450-y (2020).

38 Musallam, K. M. *et al.* Preoperative anaemia and postoperative outcomes in non-cardiac surgery: a retrospective cohort study. *The Lancet* **378**, 1396-1407, doi:10.1016/S0140-6736(11)61381-0 (2011).

39 Dunne, J. R., Malone, D., Tracy, J. K., Gannon, C. & Napolitano, L. M. Perioperative anemia: an independent risk factor for infection, mortality, and resource utilization in surgery. *J Surg Res* **102**, 237-244, doi:10.1006/jsre.2001.6330 (2002).

40 Kanemasa, H. *et al.* The immunoregulatory function of peripheral blood CD71+ erythroid cells in systemic-onset juvenile idiopathic arthritis. *Scientific Reports* **11**, 14396, doi:10.1038/s41598-021-93831-3 (2021).

41 Hill, D. L. *et al.* Immune system development varies according to age, location, and anemia in African children. *Sci Transl Med* **12**, doi:10.1126/scitranslmed.aaw9522 (2020).
42 Peter, V. *et al.* Normal and pathological erythropoiesis in adults: from gene regulation to targeted treatment concepts. *Haematologica* **103**, 1593-1603, doi:10.3324/haematol.2018.192518 (2018).
43 Han, Y. *et al.* Tumor-Induced Generation of Splenic Erythroblast-like Ter-Cells Promotes Tumor Progression. *Cell* **173**, 634-648.e612, doi:10.1016/j.cell.2018.02.061 (2018).
44 Hou, Y. *et al.* Radiotherapy and immunotherapy converge on elimination of tumor-promoting erythroid progenitor cells through adaptive immunity. *Science Translational Medicine* **13**, eabb0130, doi:10.1126/scitranslmed.abb0130 (2021).
45 Huang, P. *et al.* Putative regulators for the continuum of erythroid differentiation revealed by single-cell transcriptome of human BM and UCB cells. *Proceedings of the National Academy of Sciences* **117**, 12868-12876, doi:10.1073/pnas.1915085117 (2020).
46 Dunsmore, G. *et al.* Erythroid Suppressor Cells Compromise Neonatal Immune Response against Bordetella pertussis. *The Journal of Immunology*, ji1700742, doi:10.4049/jimmunol.1700742 (2017).
47 Paulson, R. F., Ruan, B., Hao, S. & Chen, Y. Stress Erythropoiesis is a Key Inflammatory Response. *Cells* **9**, doi:10.3390/cells9030634 (2020).
48 Greten, F. R. & Grivennikov, S. I. Inflammation and Cancer: Triggers, Mechanisms, and Consequences. *Immunity* **51**, 27-41, doi:10.1016/j.immuni.2019.06.025 (2019).
49 Dunsmore, G. *et al.* Lower Abundance and Impaired Function of CD71+ Erythroid Cells in Inflammatory Bowel Disease Patients During Pregnancy. *J Crohns Colitis* **13**, 230-244, doi:10.1093/ecco-jcc/jjy147 (2019).
50 Libregts, S. F. *et al.* Chronic IFN-γ production in mice induces anemia by reducing erythrocyte life span and inhibiting erythropoiesis through an IRF-1/PU.1 axis. *Blood* **118**, 2578-2588, doi:10.1182/blood-2010-10-315218 (2011).
51 de Bruin, A. M., Voermans, C. & Nolte, M. A. Impact of interferon-γ on hematopoiesis. *Blood* **124**, 2479-2486, doi:10.1182/blood-2014-04-568451 (2014).
52 Zhang, J. *et al.* Rats offer a superior model of human stress erythropoiesis. *Experimental Hematology*, doi:https://doi.org/10.1016/j.exphem.2019.09.021 (2019).
53 Dev, A. *et al.* During EPO or anemia challenge, erythroid progenitor cells transit through a selectively expandable proerythroblast pool. *Blood* **116**, 5334-5346, doi:10.1182/blood-2009-12-258947 (2010).
54 Lewis, S. M., Williams, A. & Eisenbarth, S. C. Structure and function of the immune system in the spleen. *Sci Immunol* **4**, eaau6085, doi:10.1126/sciimmunol.aau6085 (2019).
55 Grzywa, T. M., Justyniarska, M., Nowis, D. & Golab, J. Tumor Immune Evasion Induced by Dysregulation of Erythroid Progenitor Cells Development. *Cancers (Basel)* **13**, doi:10.3390/cancers13040870 (2021).
56 Srikantia, S. G., Prasad, J. S., Bhaskaram, C. & Krishnamachari, K. A. Anaemia and immune response. *Lancet (London, England)* **1**, 1307-1309, doi:10.1016/s0140-6736(76)92647-7 (1976).

57 Aly, S. S., Fayed, H. M., Ismail, A. M. & Abdel Hakeem, G. L. Assessment of peripheral blood lymphocyte subsets in children with iron deficiency anemia. *BMC Pediatrics* **18**, 49, doi:10.1186/s12887-018-0990-5 (2018).

58 Pasricha, S.-R., Colman, K., Centeno-Tablante, E., Garcia-Casal, M.-N. & Peña-Rosas, J.-P. Revisiting WHO haemoglobin thresholds to define anaemia in clinical medicine and public health. *The Lancet Haematology* **5**, e60-e62, doi:https://doi.org/10.1016/S2352-3026(18)30004-8 (2018).

59 Reese, T. A. *et al.* Chitin induces accumulation in tissue of innate immune cells associated with allergy. *Nature* **447**, 92-96, doi:10.1038/nature05746 (2007).

60 Hogquist, K. A. *et al.* T cell receptor antagonist peptides induce positive selection. *Cell* **76**, 17-27, doi:10.1016/0092-8674(94)90169-4 (1994).

61 O'Connell, K. E. *et al.* Practical murine hematopathology: a comparative review and implications for research. *Comp Med* **65**, 96-113 (2015).

62 Edgar, R. C. MUSCLE: multiple sequence alignment with high accuracy and high throughput. *Nucleic Acids Res* **32**, 1792-1797, doi:10.1093/nar/gkh340 (2004).

63 Webb, B. & Sali, A. Comparative Protein Structure Modeling Using MODELLER. *Curr Protoc Bioinformatics* **54**, 5 6 1-5 6 37, doi:10.1002/cpbi.3 (2016).

64 Williams, C. J. *et al.* MolProbity: More and better reference data for improved all-atom structure validation. *Protein Sci* **27**, 293-315, doi:10.1002/pro.3330 (2018).

65 Jones, G., Willett, P., Glen, R. C., Leach, A. R. & Taylor, R. Development and validation of a genetic algorithm for flexible docking. *J Mol Biol* **267**, 727-748, doi:10.1006/jmbi.1996.0897 (1997).

66 Jain, A. N. Surflex: fully automatic flexible molecular docking using a molecular similarity-based search engine. *Journal of medicinal chemistry* **46**, 499-511, doi:10.1021/jm020406h (2003).

67 Pronk, S. *et al.* GROMACS 4.5: a high-throughput and highly parallel open source molecular simulation toolkit. *Bioinformatics* **29**, 845-854, doi:10.1093/bioinformatics/btt055 (2013).

68 M. Bradbrook, G. *et al.* X-Ray and molecular dynamics studies of concanavalin-A glucoside and mannoside complexes Relating structure to thermodynamics of binding. *Journal of the Chemical Society, Faraday Transactions* **94**, 1603-1611, doi:10.1039/A800429C (1998).

69 Malde, A. K. *et al.* An Automated Force Field Topology Builder (ATB) and Repository: Version 1.0. *J Chem Theory Comput* **7**, 4026-4037, doi:10.1021/ct200196m (2011).

70 Heshusius, S. *et al.* Large-scale in vitro production of red blood cells from human peripheral blood mononuclear cells. *Blood Advances* **3**, 3337-3350, doi:10.1182/bloodadvances.2019000689 (2019).

Figures

Figure 1. Anemia induces CECs expansion in the spleen

a, Representative plots of $CD71^+TER119^+$ CECs of total live cells in the spleens of control, anemic, and 3-days old neonatal mice. **b,** The frequency of $CD71^+TER119^+$ CECs of total splenocytes in control (n=10), control-IgG (n=7), anemic (NHA, n=13; HA-PHZ, n=9; HA-TER119, n=8), and 3-days old neonatal mice (n=5). *P* values were calculated with Kruskal-Wallis test with Dunn's post-hoc test. **c,** Numbers of $CD71^+TER119^+$ CECs in the spleens of control (n=4), anemic (NHA, n=4; HA-PHZ, n=4; HA-TER119, n=4), and neonatal (n=4) mice. *P* values were calculated with one-way ANOVA with Dunnet's post-hoc test. **d,** Percentages of $CD45.2^-$ and $CD45.2^+$ cells within CECs ($CD71^+TER119^+$) population (n=5). Representative plot of CD45 levels in CECs and $TER119^-$ cells in the spleen of NHA mouse. **e,** Gating strategy for CECs developmental stages based on CD44 expression and cells size[16]. **f,** Developmental stages of CECs in control mice (n=9), NHA mice (n=13), HA-PHZ (n=9), HA-TER119 (n=5), and neonatal mice (n=5). **g,** Representative plot of CD71 and CD45 levels in CECs in the spleen of NHA mouse and analysis of developmental stages of $CD45^+$ CECs and $CD45^-$ CECs. **h,** Percentages of $CD45^+$ CECs in different developmental stages in the spleens of NHA mice (n=5). Histograms show the fluorescence of CD45 – BV711. Red blood cells (RBCs) are presented as a negative control. **i,** Percentages of nucleated CECs (Hoechst 33342^+) in different developmental stages in the spleens of NHA mice (n=5). Histograms show the fluorescence of Hoechst 33342 – INDO-1. Red blood cells (RBCs) are presented as a negative control. Data show means ± SD. Each point in **b-d,h,i** represents data from individual mice. *n* values are the numbers of mice used to obtain the data. The source data underlying Fig.1b-d,f,h,i are provided as a Supplementary Data file.

Figure 2. Anemic mice have impaired T-cell immune response

a, Schematic presentation of the experimental setting. T-cells isolated from OT-I mice were labeled with CellTraceViolet (CTV) and adoptively transferred to anemic and healthy control mice and stimulated with OVA. **b,** Percentage of proliferating (CTV^{low}) OT-I T-cells in the spleen of NHA mice (n=8), HA-PHZ mice (n=8), and healthy controls (n=5). Histograms show the fluorescence of CTV (CellTraceViolet) – V450 of OT-I T-cells. *P* values were calculated with one-way ANOVA with Tukey's post-hoc test. **c,** Representative plot of CD71 and TER119 levels in isolated CECs. Additional plots are presented in Supplementary Fig. 4. **d,** Proliferation triggered by αCD3/αCD28 in CTV-labelled $CD4^+$ T-cells co-cultured with CECs isolated from the spleens of NHA (n=8), HA-PHZ (n=8), or HA-TER119 (n=4) mice. T-cell:CECs ratio was 1:2. Representative proliferation histograms of αCD3/αCD28-stimulated $CD4^+$ T-cells co-cultured with CECs. Histograms show the fluorescence of CTV (CellTraceViolet) – V450. *P* values were calculated with one-way ANOVA with Dunnet's post-hoc test. Data show means ± SD. Each point in **b,d** represents data from individual mice. *n* values are the numbers of mice. The source data underlying Fig. 2b,d are provided as a Supplementary Data file.

Figure 3. CECs from anemic mice express ARG2 and have high levels of ROS

a, Mean Fluorescence Intensity (MFI) of CellROX Green – FITC in CECs ($CD71^+TER119^+$) and RBCs ($CD71^-TER119^+$) of control (n=6), NHA (n=6), and HA-PHZ (n=6) mice. Histograms show representative fluorescence of CellROX Green – FITC in CECs and RBCs from the spleens of the NHA mouse. *P* values were

calculated with unpaired *t*-test. **b,** Mean Fluorescence Intensity (MFI) of CellROX Green – FITC in CECs ($CD71^+TER119^+$), $CD45^+$ CECs ($CD45^+CD71^+TER119^+$), leukocytes ($CD45^+TER119^-$), T-cells ($CD45^+CD3e^+$), and myeloid cells ($CD45^+CD11b^+$) (n=18). *P* values were calculated with Friedman's test with Dunn's post-hoc test. **c,** Percentages of $ARG2^+$ CECs in control mice (n=11), anemic mice (NHA, n=5; HA-PHZ, n=11; HA-TER119, n=11), neonatal mice (n=5), and isotype control-IgG-treated mice (control-IgG, n=7) based on intracellular staining. **d,** Mean Fluorescence Intensity (MFI) of ARG2-APC in CECs from control mice, anemic mice (NHA, HA-PHZ, HA-TER119), neonatal mice, and isotype control-IgG-treated mice (each group n=5). Histograms show the representative fluorescence of ARG2 – APC in CECs in different groups and in anti-ARG2-unstained controls. **e**, Percentages of $ARG1^+$ CECs based on intracellular staining (n=5). *P* values were calculated with one-way ANOVA with Dunnet's post-hoc test and with an unpaired *t*-test for HA-TER119. **f,** Percentages of YFP^+ CECs in reporter B6.129S4-$Arg1^{tm1Lky}$/J mice (controls n=4, NHA n=8, HA-PHZ n=8, neonatal n=5, control-IgG n=4, HA-TER119 n=8). *P* values were calculated with one-way ANOVA with Dunnet's post-hoc test and with an unpaired *t*-test for HA-TER119. **g,** Mean Fluorescence Intensity (MFI) of YFP – FITC in CECs of reporter B6.129S4-$Arg1^{tm1Lky}$/J mice in control mice (n=4), anemic (NHA n=8, HA-PHZ n=4, HA-TER119 n=8), neonatal mice (n=5) and isotype control-IgG-treated mice (n=4). *P* values were calculated with one-way ANOVA with Dunnet's post-hoc test. **h,** Representative fluorescence of ARG1 – YFP in CECs in reporter B6.129S4-$Arg1^{tm1Lky}$/J control mice and anemic mice (NHA, HA-PHZ). Background fluorescence of YFP in CECs from wild-type C57Bl/6 mice presented as a negative YFP control. **i,j,** Total arginase activity in CECs lysates (**i,** n=8) or in the supernatants from CECs cultures (**j**, n=8). *P* values were calculated with one-way

ANOVA with unpaired *t*-test. **k,l,** Percentages of ARG1^{+} CECs (**k**) isolated from the spleens of B6.129S4-Arg1^{tm1Lky}/J incubated with diluent or PHZ (100 μM for 24h) (n=3) and representative fluorescence of ARG1 – YFP (**l**). *P* values were calculated with unpaired *t*-test. Data show means ± SD. Each point in **a-g, i-k** represents data from individual mice. *n* values are the numbers of mice used to obtain the data. The source data underlying Fig. 3a-g, i-k are provided as a Supplementary Data file.

Figure 4. Phenylhydrazine targets arginase, inhibits its activity, and induces oxidative damage

a, Inhibition curves for recombinant human ARG1 and ARG2, and IC_{50} values for PHZ (n=2) and 2(S)-amino-6-boronohexanoic acid (ABH). **b,** NO production from CECs and whole splenocytes population isolated from NHA (n=4) and HA-PHZ (n=4) mice. *P*-values were calculated with an unpaired *t*-test. **c,** The electrostatic surface potential of the human ARG1. The potential was calculated with APBS and projected onto the molecular surface of the protein. The figure was prepared with UCSF Chimera. **d,** Carbonylation of ARG1 in the presence of PHZ (n=3). Representative blot (left) and densitometric analysis done with ImageJ software (right). The negative lane represents ARG1 precipitates treated with 2N HCl alone. *P*-values were calculated with Ordinary one-way ANOVA with Dunnett's multiple comparisons test. Data show means ± SD. Each point in **b** represents data from individual mice. *n* values are the numbers of mice used to obtain the data or the number of biological replicates of *in vitro* experiments. The source data underlying Fig.4a, 4b, 4d are provided as a Supplementary Data file.

Figure 5. CECs degrade L-Arg and produce ROS leading to the suppression of T-cells

a, Proliferation and surface markers in αCD3/αCD28-stimulated $CD4^+$ T-cells co-cultured with CECs isolated from NHA mice (n=4) at a ratio 1:2 (T-cells:CECs). *P*-value was calculated with an unpaired t-test. **b**, Effects of ARGi (OAT-1746, 500 nM) and ROSi (N-acetylcysteine, 100 μM) on the proliferation of αCD3/αCD28-stimulated $CD4^+$ T-cells co-cultured with CECs isolated from the spleens of NHA mice (n=4) at a ratio 1:2 (T-cells:CECs). Representative proliferation histograms of αCD3/αCD28-stimulated $CD4^+$ T-cells co-cultured with CECs in the presence of ARGi or ROSi. Histograms show the fluorescence of CTV (CellTraceViolet) – V450. *P*-value was calculated with one-way ANOVA with Bonferroni's post-hoc test. **c,** Effects of L-arginine supplementation (1000 μM) or ARGi (OAT-1746, 500 nM) on the proliferation of αCD3/αCD28-stimulated $CD4^+$ T-cells cultured in full medium or in CECs-conditioned medium (CM) (n=3). *P*-value was calculated with one-way ANOVA with Bonferroni's post-hoc test. **d**, Proliferation of αCD3/αCD28-stimulated $CD4^+$ T-cells co-cultured with total CECs population or with nucleated CECs (nCECs) isolated using density-gradient centrifugation from NHA mice (n=5) at a ratio 1:2 (T-cells:CECs). Histograms show the fluorescence of CTV (CellTraceViolet) – V450. *P*-value was calculated with repeated measures ANOVA with Holm-Sidak's post-hoc test. **e,f,** Proliferation of αCD3/αCD28-stimulated $CD4^+$ T-cells (**e**) or $CD8^+$ T-cells (**f**) co-cultured with CECs isolated from NHA mice (n=4) at a ratio 1:10 (T-cells:CECs). *P*-value was calculated with paired t-test. **g,** Arginase activity of the splenocytes lysate of control and anemic mice calculated per μg of total protein based on bicinchoninic acid (BCA) protein assay. *P*-value was calculated with an unpaired t-test. **h,** The level of ARG1 and ARG2 in the splenocytes lysate of control (n=4) and

anemic mice (n=4). β-actin showed as a loading control. **i,j** Relative density of ARG1 (**i**) and ARG2 (**j**) compared to β-actin. *P*-value was calculated with an unpaired t-test. **k,l,** The level of CD3ζ in $CD4^+$ (**k**) and $CD8^+$ (**l**) T-cells in the spleen of control (n=4) and anemic mice (n=4) based on intracellular staining. *P*-value was calculated with an unpaired t-test. **m,n,** The levels of CD3ζ in $CD4^+$ (**m**) and $CD8^+$ (**n**) αCD3/αCD28-stimulated T-cells in the presence of CECs isolated from NHA mice (n=4) based on intracellular staining. *P*-value was calculated with one-way ANOVA with Bonferroni's post-hoc test. Data show means ± SEM (a-f, m,n) or means ± SD (h,i-l). Each point in **a-g, i-n** represents data from individual mice. *n* values are the numbers of mice used to obtain the data or the number of biological replicates in *in vitro* experiments. The source data underlying Fig. 5a-n are provided as a Supplementary Data file.

Figure 6. CECs from $Arg2^{-/-}$ mice have impaired immunoregulatory properties

a, The levels of CD3ζ in spleen $CD4^+$ (**a**) and $CD8^+$ (**b**) T-cells in control (n=4) and anemic mice (n=4) based on intracellular staining. Histograms show the fluorescence of CD3ζ – FITC in $CD4^+$ (**a**) and $CD8^+$ (**b**) T-cells. *P*-values were calculated with one-way ANOVA with Tukey's post-hoc test. **c,** Proliferation of αCD3/αCD28-stimulated $CD4^+$ T-cells co-cultured with CECs isolated from NHA *Arg2*$^{-/-}$ mice or NHA wild-type *Arg2*$^{+/+}$ mice at a 1:4 ratio (T-cells:CECs). Representative proliferation histograms of αCD3/αCD28-stimulated $CD4^+$ T-cells co-cultured with CECs isolated from *Arg2*$^{-/-}$ mice or wild-type *Arg2*$^{+/+}$ mice in the presence of ARGi or ROSi. Histograms show the fluorescence of CTV (CellTraceViolet) – V450. *P*-values were calculated with one-way ANOVA with Bonferroni's post-hoc test. Data show means ± SD (**a,b**) or means ± SEM (**c**). Each point in **a-c** represents data from individual mice. *n* values are the numbers of mice used to obtain the data or the number of biological

replicates in *in vitro* experiments. The source data underlying Fig. 6a-c are provided as a Supplementary Data file.

Figure 7. CECs expand in the blood of anemic patients and suppress T-cells response

a, Percentages of live $CD71^{+}CD235a^{+}$ CECs in the whole blood of non-anemic (controls, n=42) and anemic patients (n=41). *P*-value was calculated with the Mann-Whitney test. **b,** Representative dot plots of CECs in the blood of non-anemic and anemic patients. **c,** CECs count per µl of blood in controls (n=42) and anemic patients (n=41). *P*-value was calculated with the Mann-Whitney test. **d,** Correlation of the number of CECs per µl of blood and hemoglobin concentration (n=82). The correlation was calculated with Spearman r. **e,** CECs count per µl of blood in non-anemic controls (n=42) and patients with mild (n=7), moderate (n=32), and severe (n=2) anemia. *P*-values were calculated with Kruskal-Wallis test with Dunn's post-hoc test. **f,g,** Percentages of CECs in the fraction of peripheral blood mononuclear cells (PBMC) in controls (n=12) and anemic patients (n=13) (**f**) and representative dot plots of CECs (**g**). *P*-value was calculated with the Mann-Whitney test. **h,** PBMCs of controls (n=12) and anemic patients (n=13) were stimulated with αCD3/αCD28 for 12h in the presence of a protein transport inhibitor. IFN-γ levels were determined by intracellular staining. *P*-values were calculated with an unpaired *t*-test. **i,** Representative plots of IFN-γ levels in unstimulated or αCD3/αCD28-stimulated $CD3\varepsilon^{+}$ T-cells from PBMCs of anemic patients or non-anemic controls. Isotype control-stained cells are shown as a negative control. Data show means ± SD. Each point in **a,c-f,h** represents data from individual patients. *n* values are the numbers of

patients used to obtain the data or the number of biological replicates in *in vitro* experiments. The source data underlying Fig.7a, 7c-f, 7h are provided as a Supplementary Data file.

Figure 8. CECs from human bone marrow express ARG1 and ARG2 and suppress T-cells proliferation

a, Representative plots of $CD71^+$ and $CD235^+$ CECs in the aspirate of human bone marrow of total live cells. **b,** Percentages of $ARG1^+$ and $ARG2^+$ CECs in the human bone marrow based on intracellular staining. **c,** Mean Fluorescence Intensity (MFI) of ARG1-PE and ARG2-APC in CECs. **d,** Representative histograms of ARG1 and ARG2 levels in CECs from human bone marrow. Fluorescence-minus-one (FMO) is shown as unstained controls. **e,f,** Proliferation triggered by αCD3/αCD28 of CTV-labelled $CD4^+$ (**e**) and $CD8^+$ (**f**) T-cells co-cultured with CECs isolated from the human bone marrow. T-cell to CECs ratio was 1:2 (n=9). The proliferation of T-cells in co-culture with CECs was calculated as a percentage of maximum proliferation (100%) of T-cells that was triggered by αCD3/αCD28 antibodies and cultured without CECs. Representative histograms shows CTV – BV421 fluorescence of $CD4^+$ (**e**) or $CD8^+$ (**f**) T-cells co-cultured with CECs at a 1:2 ratio in the presence of ARGi (OAT-1746, 500 nM). *P*-values were calculated with Friedman's test with Dunn's post-hoc test. Data show means ± SD (**b,c**) or means ± SEM (**e,f**). *n* values are the numbers of individual patients used to obtain the data or the number of biological replicates in *in vitro* experiments. The source data underlying Fig.8b, 8c, 8e, 8f are provided as a Supplementary Data file.

Figure 9. Erythroleukemia-derived erythroid cell lines suppress T-cells in an ARG- and ROS-dependent mechanism

a, The levels of CD71 and CD235a in erythroleukemia-derived erythroid cell lines. **b-d,** Proliferation of CTV-labelled $CD4^+$ T-cells triggered by αCD3/αCD28 co-cultured with K562 (**b**), HEL92.1.7 (**c**) and TF-I (**d**) erythroid cell lines at different ratios (T-cells:CECs) (n=3). *P*-values were calculated with repeated measures ANOVA with Dunnett's post-hoc test. **e,** Representative histograms of CTV – BV421 fluorescence of $CD4^+$ T-cells co-cultured with erythroid cells at a 1:2 ratio in the presence of ARGi (OAT-1746, 1.5 μM) and ROSi (NAC, 200 μM) (n=2). Statistical analyses are provided in Supplementary Fig. 18a. **f-h,** Proliferation of CTV-labelled $CD8^+$ T-cells triggered by αCD3/αCD28 co-cultured with K562 (**f**), HEL92.1.7 (**g**), or TF-I (**h**) erythroid cells at different ratios (n=3). P-values were calculated with repeated measures ANOVA with Dunnett's post-hoc test. **i,** Representative histograms of CTV – BV421 fluorescence of $CD8^+$ T-cells co-cultured with erythroid cell lines at a 1:2 ratio in the presence of ARGi (OAT-1746, 1.5 μM) and ROSi (NAC, 200 μM) (n=2). Statistical analyses are provided in Supplementary Fig. 18b. Data show means ± SEM. *n* values are the numbers of biological replicates in *in vitro* experiments. The source data underlying Fig.9b-d, 9f-h are provided as a Supplementary Data file.

Figure 10. Suppression of T-cells is a general feature of erythroid cells that diminishes with CECs maturation

a, Representative plot of isolated CECs differentiated from PBMCs. **b,c,** Proliferation of CTV-labelled $CD4^+$ (**b**) and $CD8^+$ (**c**) T-cells triggered by αCD3/αCD28 co-cultured with CECs differentiated from PBMCs (n=4). *P*-values were calculated with one-way

ANOVA with Dunnett's post-hoc test. **d,** Representative density plots of CECs differentiation from PBMCs based on CD71 and CD235a expression. **e,** Proliferation of CTV-labelled $CD4^+$ triggered by αCD3/αCD28 co-cultured with CECs-PBMCs at different developmental stages at 1:4 ratio. **f,g,** Relative proliferation of $CD4^+$ (**f**) and $CD8^+$ (**g**) T-cells co-cultured with CECs-PBMCs at different time points at a 1:4 ratio. *P*-values were calculated with one-way ANOVA with Bonferroni's post-hoc test. **h,i,j,** Levels of CD71 (**h**), CD235a (**i**), and CD49d (**j**) during erythroid differentiation from PBMCs. Data show means ± SD. Each point in **b,c, f-j** represents data from individual patients. *n* values are the numbers of individual patients used to obtain the data or the number of biological replicates in *in vitro* experiments. The source data underlying Fig.10b, 10c, 10f-j are provided as a Supplementary Data file.

1443

Figure 1.

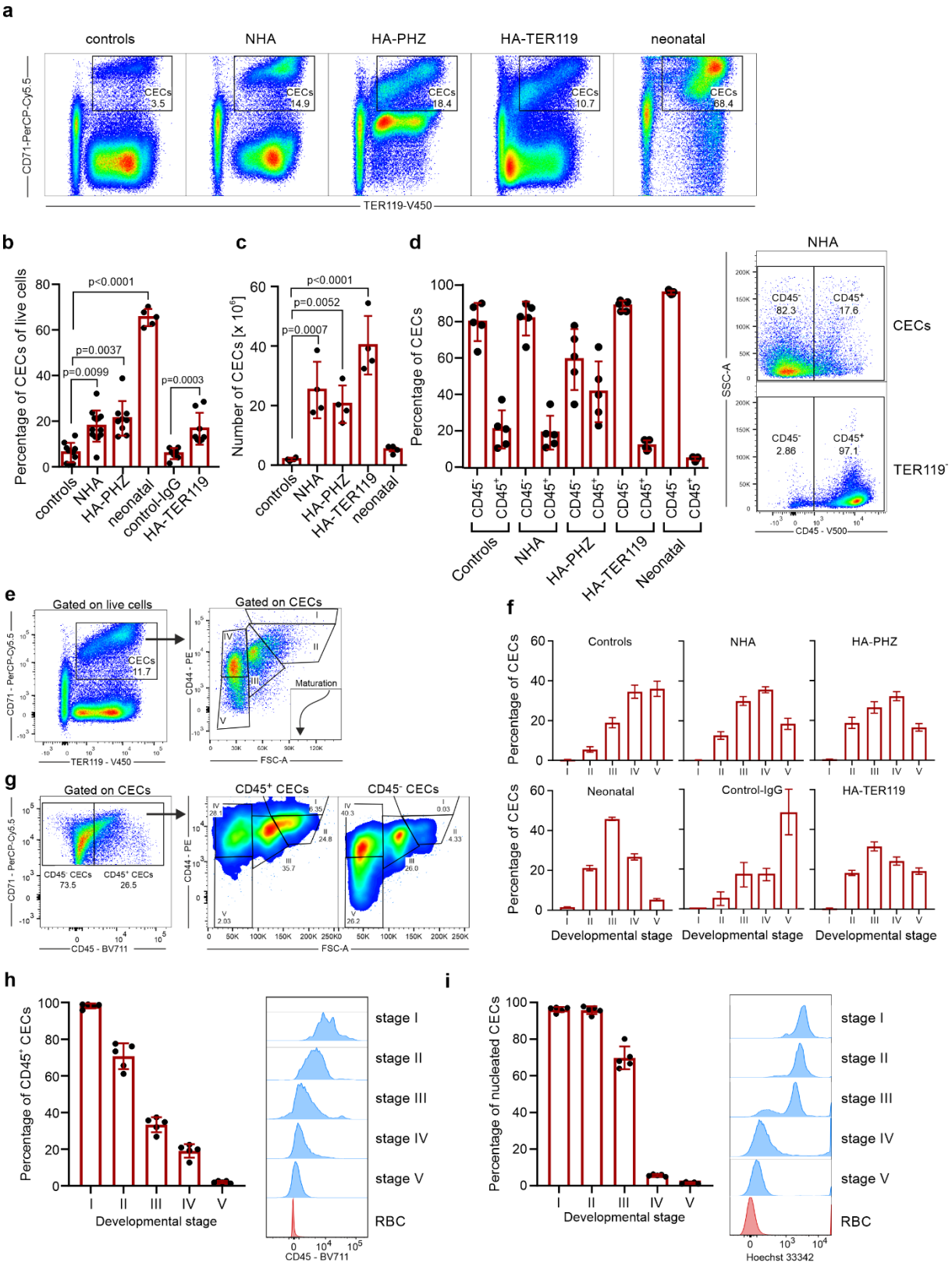

1444

1445

1446

Figure 2.

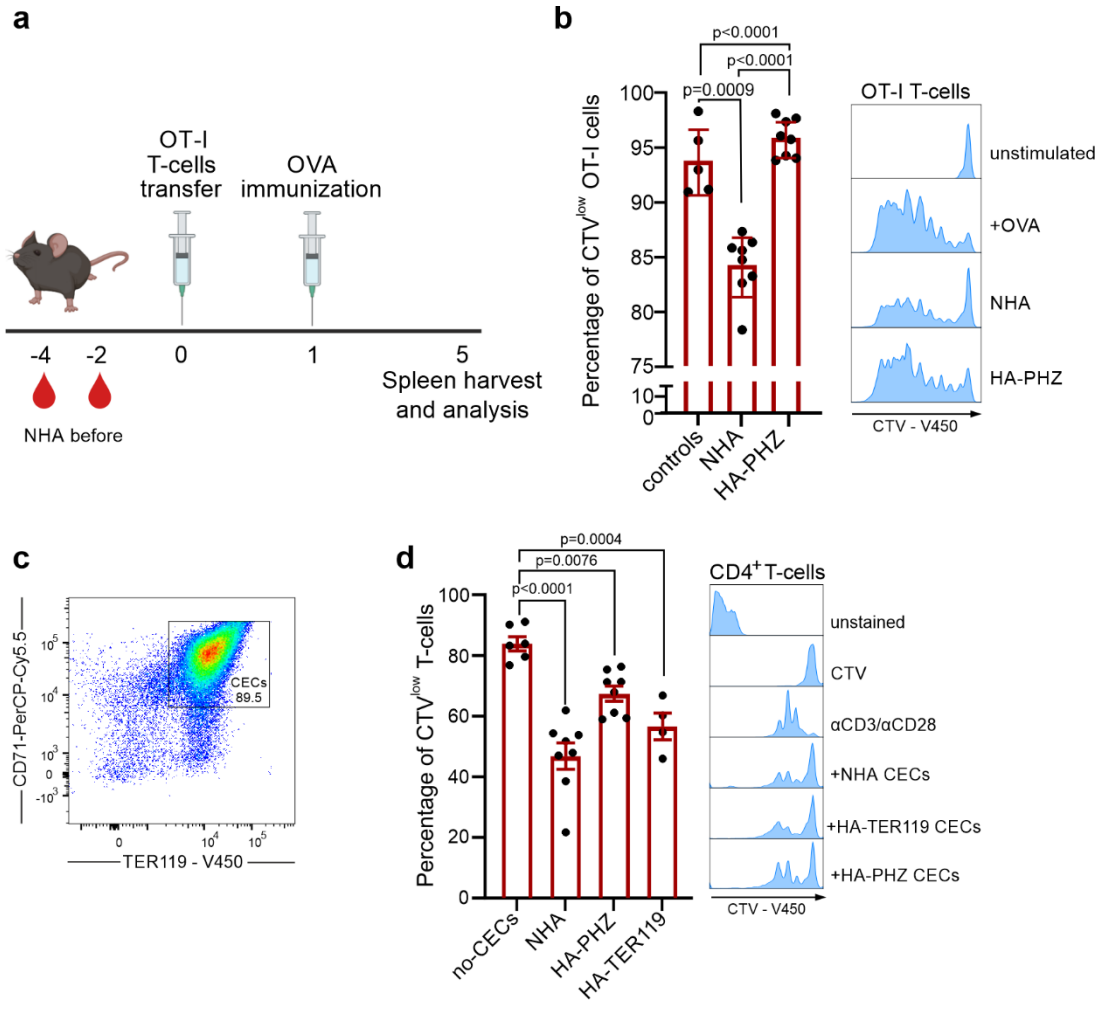

1447

1448

1449

Figure 3.

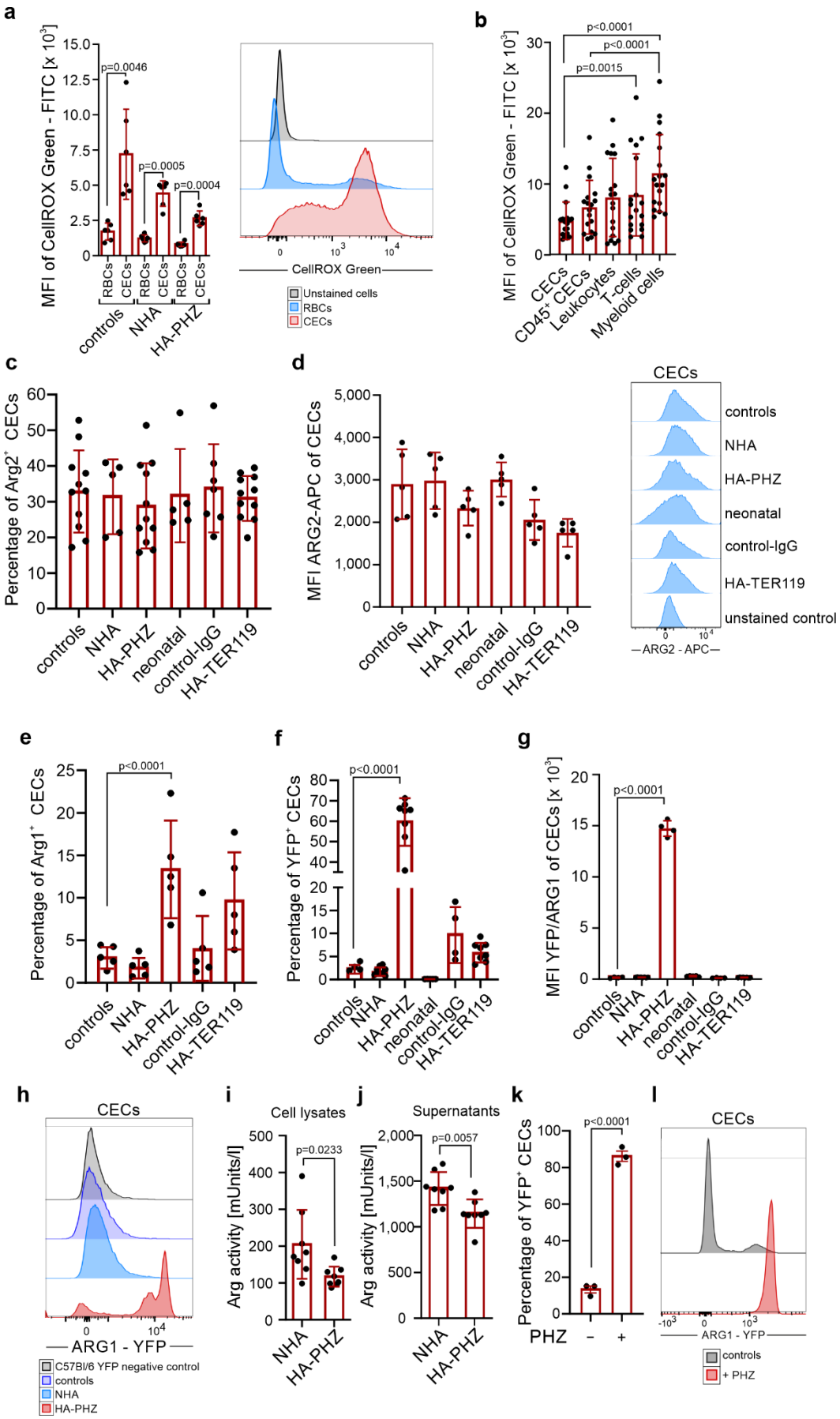

1450

1451

Figure 4.

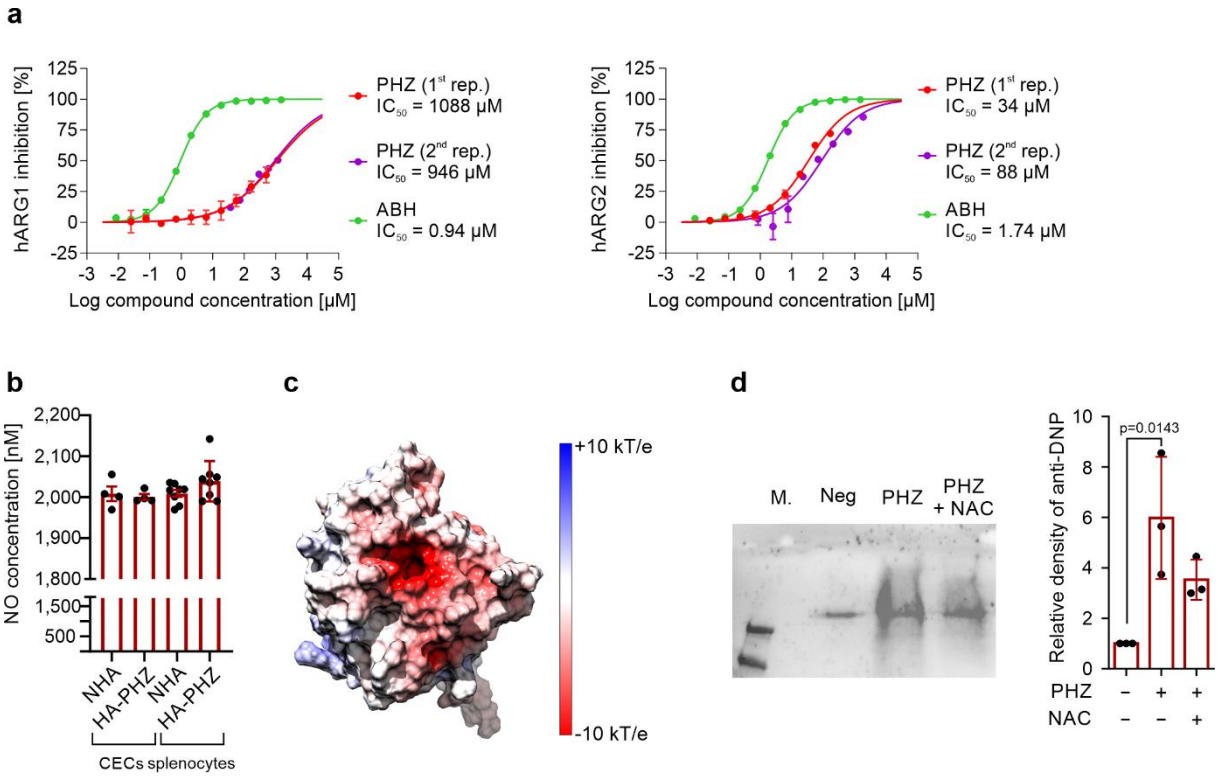

1452

1453

1454

Figure 5.

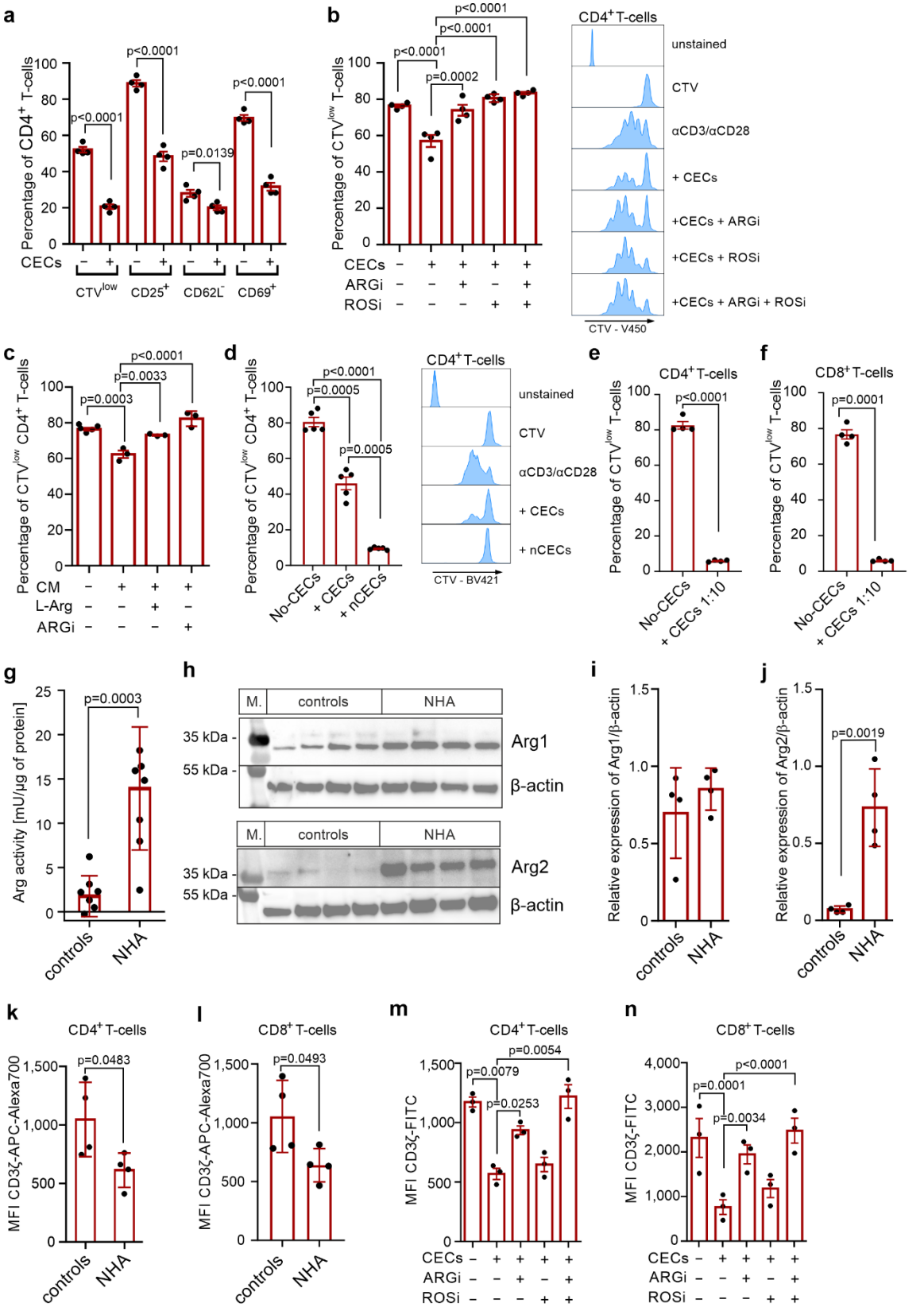

1455

1456

1457

Figure 6.

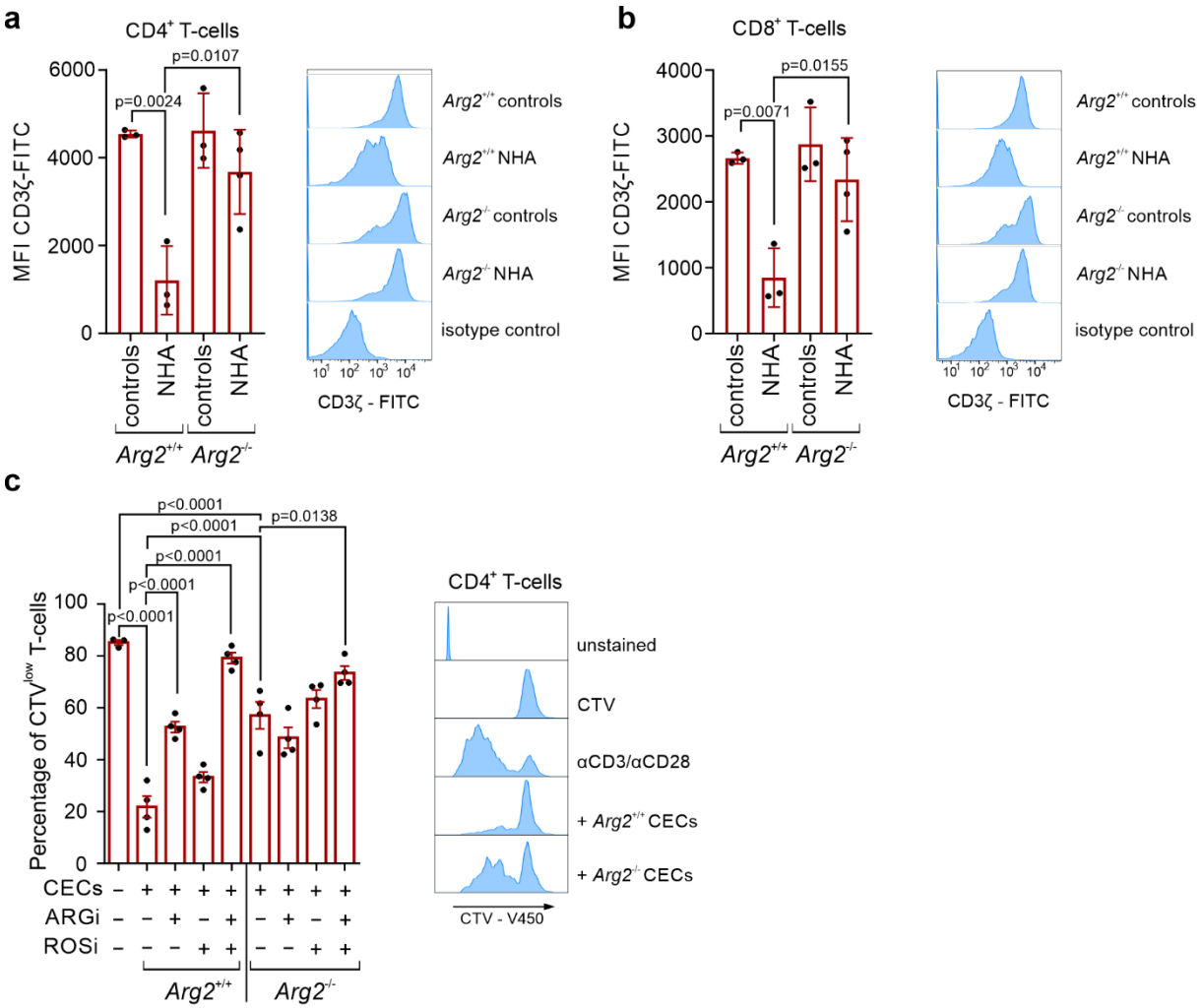

1458

1459

1460

Figure 7.

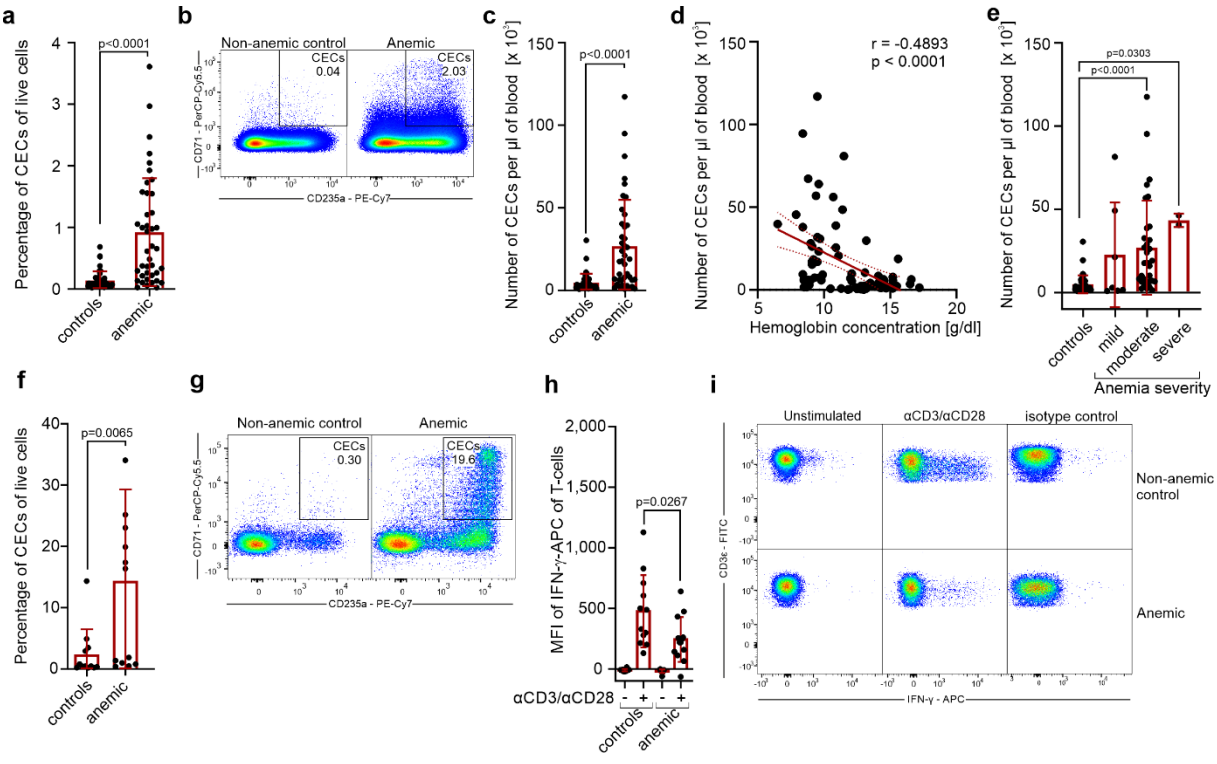

1461

1462

1463

Figure 8.

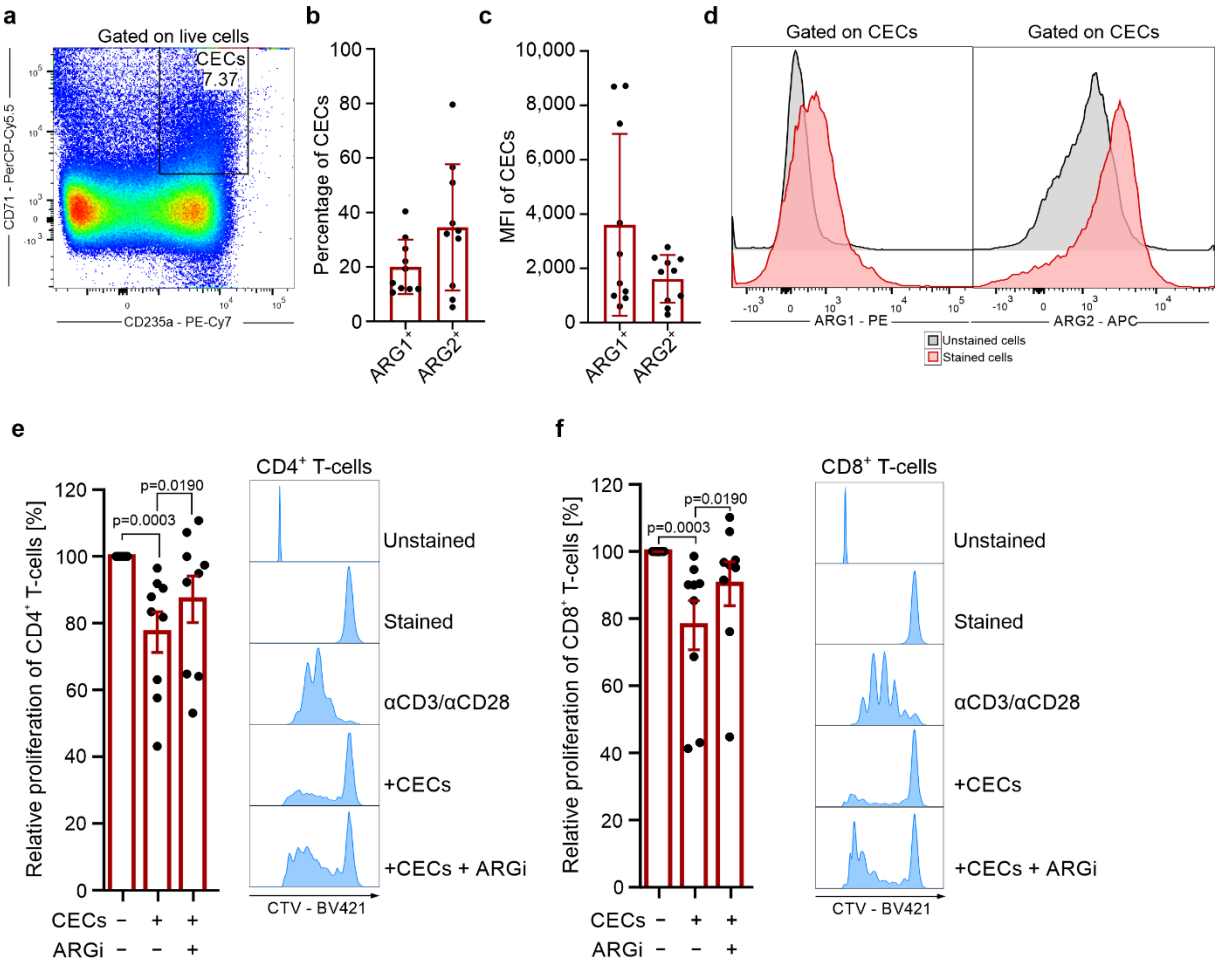

1464

1465

1466

Figure 9.

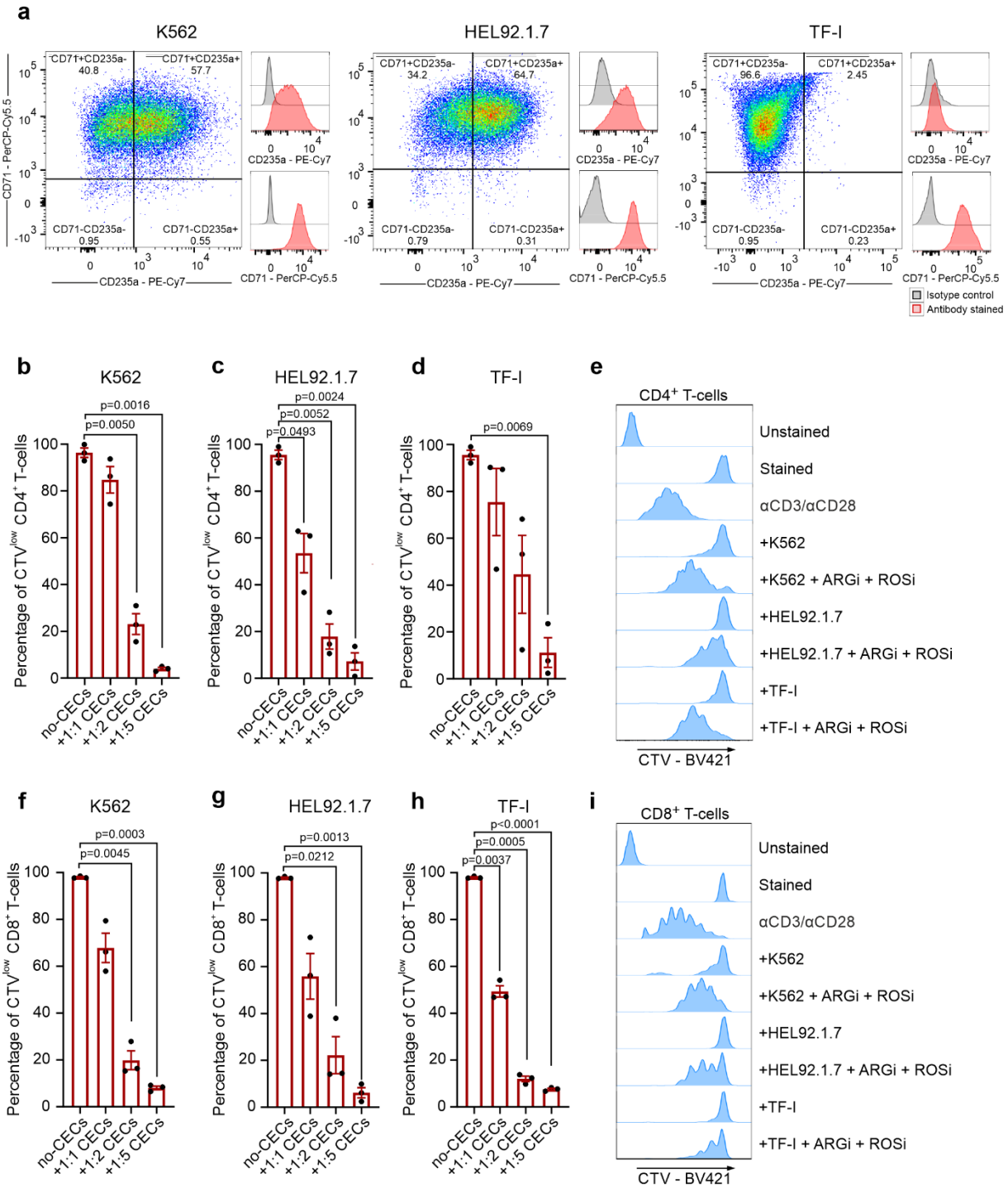

1467

1468

1469

Figure 10.

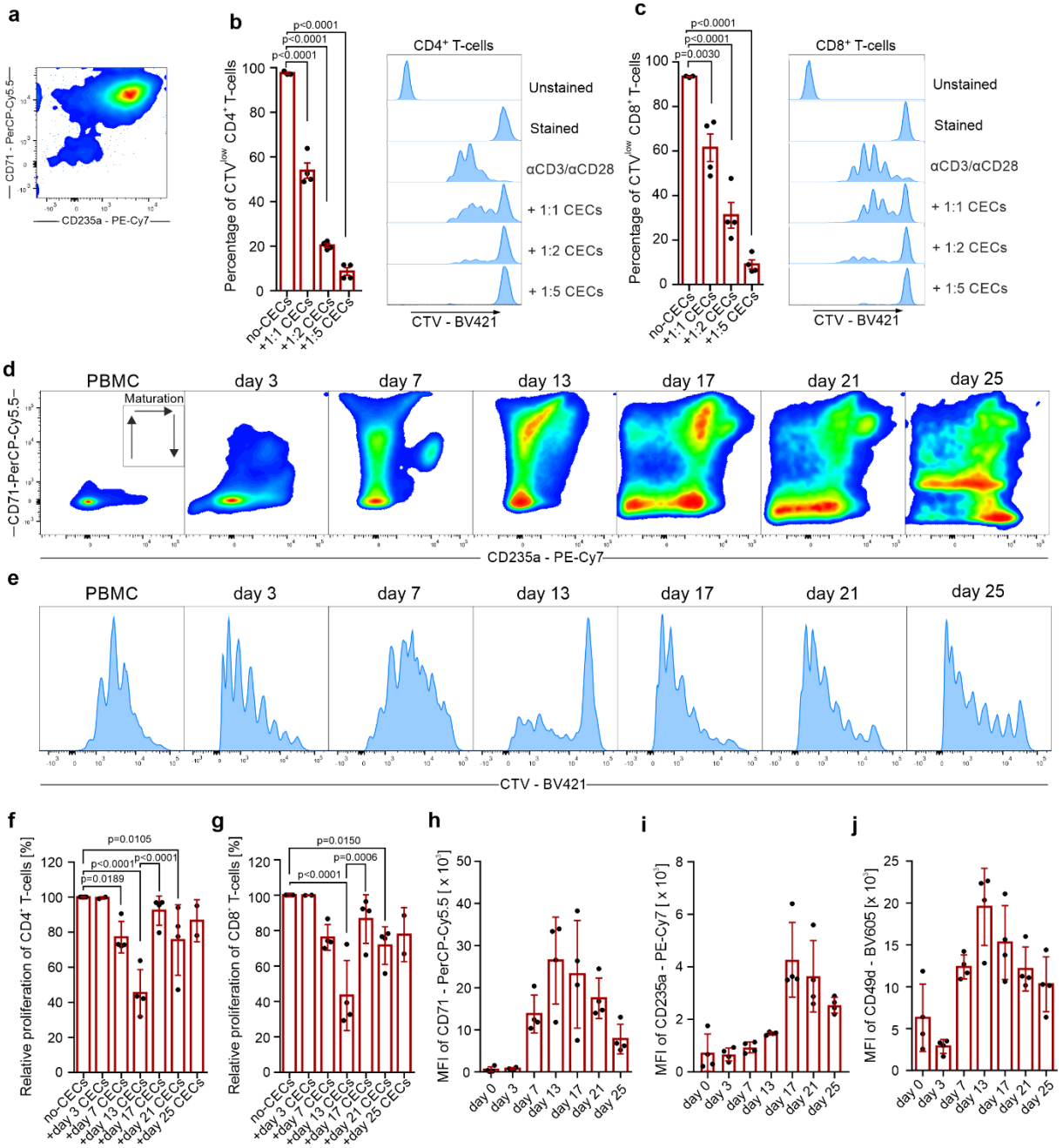

1470

1471

1472